Q. J. R. Meteorol. Soc. (1991), **117**, pp. 715–747 551.551.8:551.515.11:551.589.1(262):551.465.73

A diagnostic study of winter diabatic heating in the Mediterranean in relation to cyclones

By Y. SHAY-EL and P. ALPERT

Raymond and Beverly Sackler Faculty of Exact Sciences, Department of Geophysics and Planetary Sciences, Tel Aviv University, Ramat Aviv 69978, *Israel*

(Received 2 July 1990, revised 4 February 1991)

SUMMARY

Diabatic heating and net condensation rates during winter are calculated over the Mediterranean and surrounding areas from the 1982–88 ECMWF initialized analyses using the residual method for the heat and moisture budgets. The steady-state contributions over the Mediterranean are found to be prominent as in the tropics, but contrary to the case of the tropics the transients' contributions in the Mediterranean, attributed to cyclonic activity, are not at all negligible.

A composite Cyprus low was constituted from 67 typical cyclones in the eastern Mediterranean. The diabatic heating and net condensation distribution indicate vigorous sea fluxes especially in the lee of the Turkish mountains over the Aegean Sea where the air–sea contrast is maximized. In contrast with other regions, the maximum in the vertical profile of diabatic heating due to latent heat release is found at a lower altitude of about 850 hPa. It is suggested that this fact has important implications in modelling Mediterranean cyclones.

1. INTRODUCTION

Cyclone studies of the northern hemisphere have shown the Mediterranean to be highly cyclogenetic, particularly in winter (Petterssen 1956). Recently Alpert *et al.* (1990a) performed an objective climatological analysis of the Mediterranean cyclones based on the ECMWF analyses for 1982–87, and compared the eastern and western cyclonic centres. They found strong day-to-night and seasonal variation in both the cyclone frequencies and their geographic location, which were attributed to the strong thermal effect of the sea. This was particularly noticeable in the eastern Mediterranean. Also, vertical cross-sections of averaged winter vorticity indicated relatively low tropospheric maxima at about 850 hPa in the western region, tending to be near the sea surface over the warmer eastern Mediterranean. It has therefore been argued that the diabatic sources, i.e. sensible and latent heat fluxes, play a central role in cyclone dynamics over the Mediterranean. In addition, studies by Billing *et al.* (1983), Ernst and Matson (1983), Mayengon (1984), Rasmussen and Zick (1987) and Alpert (1984) indicated that polar-low-type cyclonic structures in the satellite pictures sometimes even have an associated hurricane eye typical of tropical storms. In this type of Mediterranean low, just as in the case of the regular polar lows of northern latitudes, the aforementioned studies provide indications of the major role of the latent and sensible heat fluxes from the warm sea to the relatively cold air above. A CISK-type process for eastern Mediterranean cyclones during early winter polar outbreaks was also suggested by Alpert (1984) and Alpert and Reisin (1986).

The purpose of the present study is to estimate quantitatively the magnitudes of the diabatic sources based on the ECMWF initialized data-sets for the period 1982–88. After introducing the method and basic equations (section 2) and the description of the data-set (section 3) the averaged winter distribution of diabatic heating and net condensation are discussed (section 4). As these diabatic terms seem to be much stronger during cyclonic events, their distribution is further investigated for the superposition of 67 Cyprus lows (section 5). In section 6 a summary and the main conclusions are presented.

2. Basic equations

(a) *Equations*

Two conservation equations are employed, one for the thermodynamic energy and the other for the moisture budget. The diabatic heating and net condensation are calculated as the residuals in the two balance equations respectively. The thermodynamic energy equation is given in isobaric coordinates per unit mass by

$$c_p \frac{\partial T}{\partial t} = - c_p \mathbf{V} \cdot \nabla T - c_p \left(\frac{p}{p_0}\right)^{\kappa} \frac{\partial \theta}{\partial p} \omega + H_T \tag{1}$$

$$(S_T) \qquad (HA_T) \qquad (VM_T)$$

where

S_T is the storage term, HA_T the horizontal advection term, VM_T the vertical motion term, and H_T the diabatic term.

The vertical motion term VM_T is the sum of the vertical advection $(-c_p\omega(\partial T/\partial p))$ and the adiabatic heating $(RT\omega)/p$. Similarly the moisture balance equation is written as

$$-L \frac{\partial q}{\partial t} = L\mathbf{V} \cdot \nabla q + L\omega \frac{\partial q}{\partial p} + H_q \tag{2}$$

$$(S_q) \qquad (HA_q) \qquad (VM_q)$$

where H_q is the net condensation, i.e. condensation minus evaporation. Common nomenclature is used here and a full list of symbols and constants is given in Appendix I. The diabatic heating and net condensation H_T, H_q were calculated as residuals in Eqs. (1) and (2), (Yanai *et al.* 1973; Kasahara *et al.* 1987).

Following Yanai *et al.* (1973) or Kuo and Anthes (1984a) H_T, H_q can be written explicitly as

$$H_T = -c_p \left\{ \mathrm{div}\langle T_1 \mathbf{V}_1 \rangle - \left(\frac{p}{p_0}\right)^{\kappa} \frac{\partial \langle T_1 \omega_1 \rangle}{\partial p} \right\} + Q_R + L(\langle c \rangle - \langle e \rangle) \tag{3}$$

$$H_q = L \left\{ \mathrm{div}\langle q_1 \mathbf{V}_1 \rangle + \frac{\partial \langle q_1 \omega_1 \rangle}{\partial p} \right\} + (\langle c \rangle - \langle e \rangle) \tag{4}$$

where Q_R is the radiative heating, c and e condensation and evaporation respectively. The angular brackets indicate a horizontal average over a grid interval and the subscript 1 stands for subgridscale perturbations. Hence, the first two terms on the right-hand side of Eqs. (3) and (4) are the contributions due to subgridscale processes like boundary-layer fluxes, cumulus convection and horizontal diffusion. Since several processes may be responsible for the diabatic heating and the net condensation as shown in Eqs. (3) and (4), it may not be completely clear, through the residual method, what physical process is contributing in each case. The present approach, however, which analyzes both H_T and H_q in conjunction with the local circumstances will facilitate the understanding of the prevailing diabatic processes in each instance.

(b) *Method of solution*

Finite difference methods are used to estimate the terms S, HA and VM in Eqs. (1) and (2), while H_T and H_q are obtained as residuals. The storage term is calculated by a forward method with a time-interval of 12 h. The horizontal derivatives are estimated by

central differences of the fourth order, while vertical differences are calculated by weighted central differences as:

$$\left.\frac{\partial F}{\partial p}\right|_{p_0} = \frac{F_{p_1} - F_{p_0}}{p_1 - p_0} \cdot \frac{p_0 - p_{-1}}{p_1 - p_{-1}} + \frac{F_{p_0} - F_{p_{-1}}}{p_0 - p_{-1}} \cdot \frac{p_1 - p_0}{p_1 - p_{-1}} \tag{5}$$

where $p_{-1} < p_0 < p_1$ and F is any variable. Near the boundaries the order of the derivatives drops.

In section 4 we discuss the winter averaged equations where winter is defined as December, January and February for 1982–88. Each term in Eqs. (1) and (2) is resolved into a steady-state term and a transient term denoted by superscripts 0 and 1 respectively. Equations (1) and (2) then yield

$$c_p \frac{\partial \overline{T}}{\partial t} = HA_T^0 + VM_T^0 + HA_T^1 + VM_T^1 + \overline{H}_T \tag{6}$$

$$-L \frac{\partial \overline{q}}{\partial t} = HA_q^0 + VM_q^0 + HA_q^1 + VM_q^1 + \overline{H}_q \tag{7}$$

where a bar over a symbol indicates a time average and

$$\begin{aligned} HA_T^0 &= -c_p \overline{\mathbf{V}} \cdot \nabla \overline{T} \\ HA_T^1 &= \overline{HA}_T - HA_T^0 = -c_p(\overline{\mathbf{V} \cdot \nabla T} - \overline{\mathbf{V}} \cdot \nabla \overline{T}). \end{aligned} \tag{8}$$

Similar expressions can be written for the other terms. This method follows Geller and Avery (1978), Kasahara *et al.* (1987), Hoskins and Sardeshmukh (1987) as well as others and makes possible the comparison of the contribution of the steady-state field with that from the transients.

It should be mentioned here that the aforementioned authors calculated the transients through the flux-form formula as, for example,

$$HA_T^1 = -c_p \nabla \cdot (\mathbf{V}^1 T^1) \tag{9}$$

but we have found larger errors in this method compared to those of the advection scheme in Eq. (8). Similar results were also reported by Holopainen and Fortelius (1986) and we have therefore preferred the advection scheme over that due to the flux-form. In section 5, where a composite Cyprus low is investigated, the aforementioned decomposition was meaningless because the selected days were not consecutive. Hence, the calculation of H_T, H_q for the composite low follows the original Eqs. (1) and (2).

In the following discussion we calculate the vertically integrated terms through the hydrostatic assumption and they are indicated by $[\,]_p$. For the diabatic heating, H_T, for instance,

$$[H_T]_p = \frac{1}{g} \int_{p_s}^{p_t} H_T \, dp \tag{10}$$

where $p_t = 100$ hPa.

Discussion of the different possible error sources in calculating H_T, H_q is given in Appendix 2. All terms in Eqs. (1) and (2) or (6) and (7) are expressed as heating rates per unit mass and can be translated into daily heating or rate of moisture loss by the following relations:

$$1 \text{ W kg}^{-1} \triangleq 86 \text{ K d}^{-1} \triangleq -35 \text{ g kg}^{-1} \text{ d}^{-1}. \tag{11}$$

The vertically integrated heating rates are given per unit area and can be translated

similarly for a 900 hPa atmospheric depth by

$$1\,\mathrm{W\,m^{-2}} \triangleq 10^{-2}\,\mathrm{K\,d^{-1}} \triangleq 3.5 \cdot 10^{-3}\,\mathrm{cm\,d^{-1}}. \tag{12}$$

The number on the right in (12) is the corresponding rainfall rate when all the heating is directly interpreted in terms of condensation to rainfall water.

3. ECMWF DATA

Initialized data-sets for the period November 1982 to December 1988 at 00 and 12 UTC with horizontal resolution of 2.5 × 2.5 degrees and seven mandatory levels (1000, 850, 700, 500, 300, 200, 100 hPa) were employed over the region (0–60°N, 0–60°E). The 4-D data assimilation system has undergone many changes with time, and has been summarized by Trenberth and Olson (1988). Two of the major modifications they have pointed out are the inclusion of diabatic nonlinear normal-mode initialization on 21 September 1982 and the higher resolution in changing from spectral model T63 to spectral model T106, as well as major changes in the physical parametrizations (clouds, convection, condensation) on 1 May 1985. Hollingsworth *et al.* (1986) examined the effects of these changes, comparing the prediction error to the observation error, and showed that they are of the same order. As the error growth in the model is about 10% for every six hours they suggested that even in sparse-data regions the model represents the real atmosphere with good accuracy. In the tropical region, however, errors may be larger than in the mid latitudes because the tropical heat and moisture fields are highly sensitive to the formulation of the physical parametrization of the model (Tiedtke *et al.* 1988).

One of the important features of the ECMWF analysis regarding the Mediterranean region is the inclusion of unconventional data from satellites (SATEMs and SATOBs), aeroplanes (AIREP, AIDS, ASDAR), buoys etc. According to Bengtsson *et al.* (1982) and Bengtsson (1988) these observations complement the data-sets particularly in otherwise data-sparse regions. Further discussion can be found in Alpert *et al.* (1990a).

4. DISTRIBUTION OF WINTER DIABATIC HEATING AND NET CONDENSATION

(*a*) *Horizontal distributions*

Figures 1 and 2 show the horizontal distributions of the vertically integrated terms of the thermodynamic and moisture-balance equations i.e. Eqs. (6) and (7), for the period December to February as based on the 1982–88 data. Regions with positive values are shaded. Figure 1(a) shows the average diabatic heating, $[\overline{H}_T]_p$, distribution. Most noticeable, compared to Fig. 2(a), are the strong positive values in the tropics due to the latent heat release, and their extension northward up to about 18°N, due primarily to the sensible heat flux. Further discussion follows later with regard to Figs. 1(b), 1(c) and 2.

In the more northern regions the radiative cooling is in general stronger, resulting in negative values for the integrated diabatic heating. Over the Mediterranean Sea and eastward at 30–50°N there are a few regions of positive diabatic heating, associated with sensible heat fluxes over the sea, latent heat release in rainy regions and also high-tropospheric heating above 200 hPa. The latter is explained by turbulent heat fluxes from the stratosphere (Hantel and Baader 1978; Chen and Baker 1986). A strong correlation exists between these regions of high diabatic heating and regions of high frequency of cyclone occurrence as reported by Alpert *et al.* (1990b). The high positive values over north-east Russia (57.5°N, 42.5°E)—maximum of above 100 $\mathrm{W\,m^{-2}}$—seem to be too

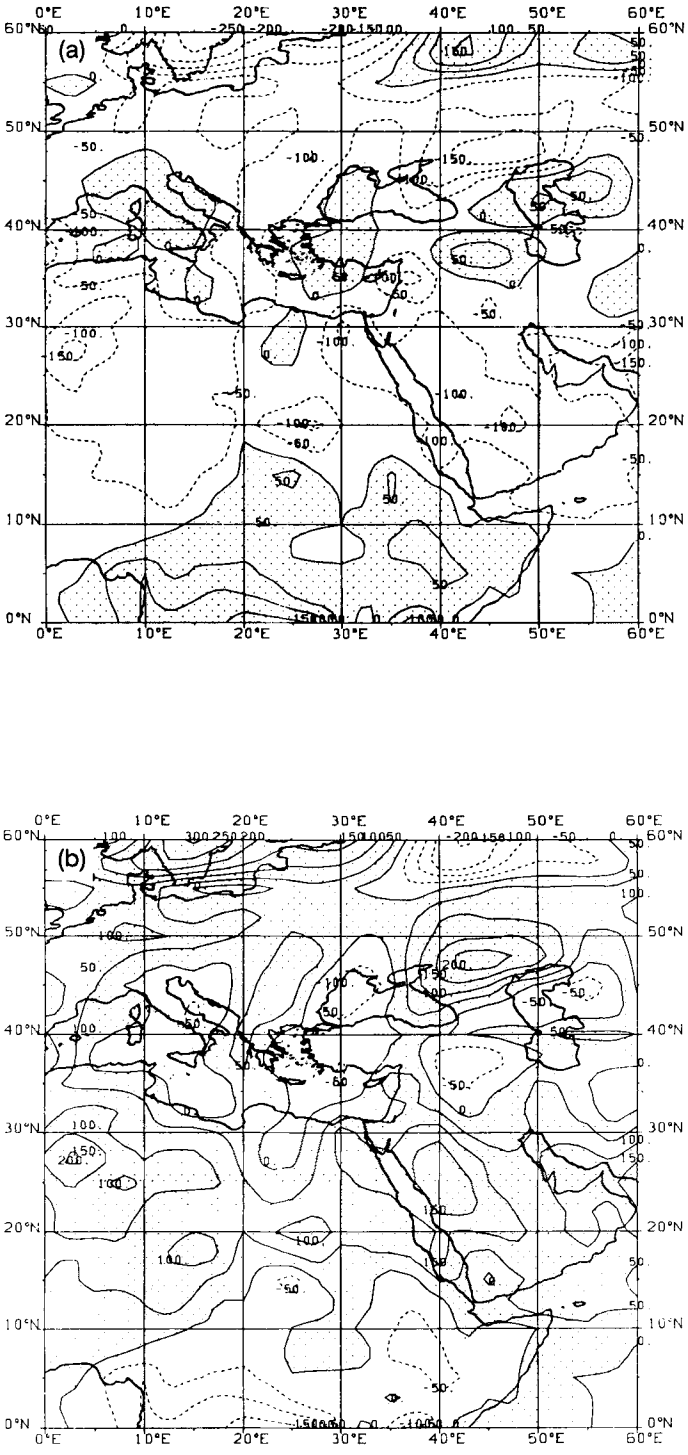

Figure 1. Horizontal distribution of the vertically integrated: (a) diabatic heating; (b) steady-state; (c) transient terms for the thermodynamic energy, Eq. (6)—for the winter (Dec.–Feb.) as based on 1982–88 ECMWF data. Positive (solid) and negative (dashed) contours are at intervals of 50 W m^{-2}. Positive-value regions are shaded.

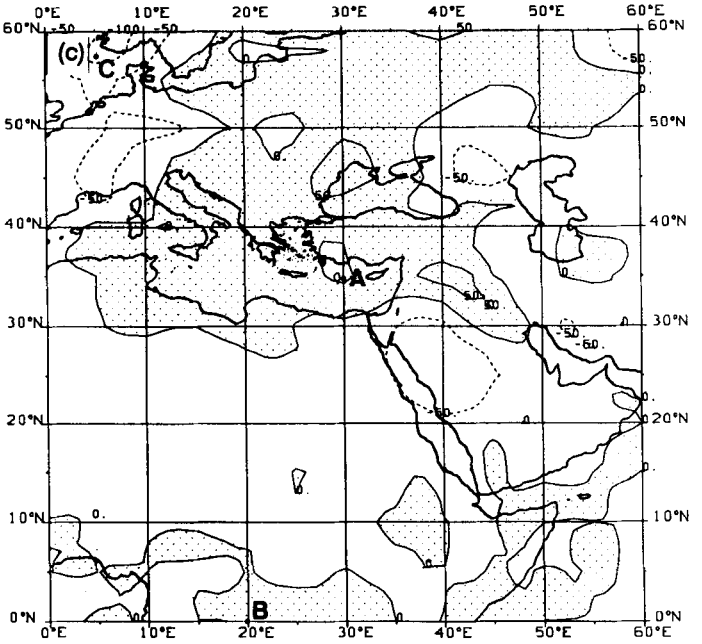

Figure 1. Continued.

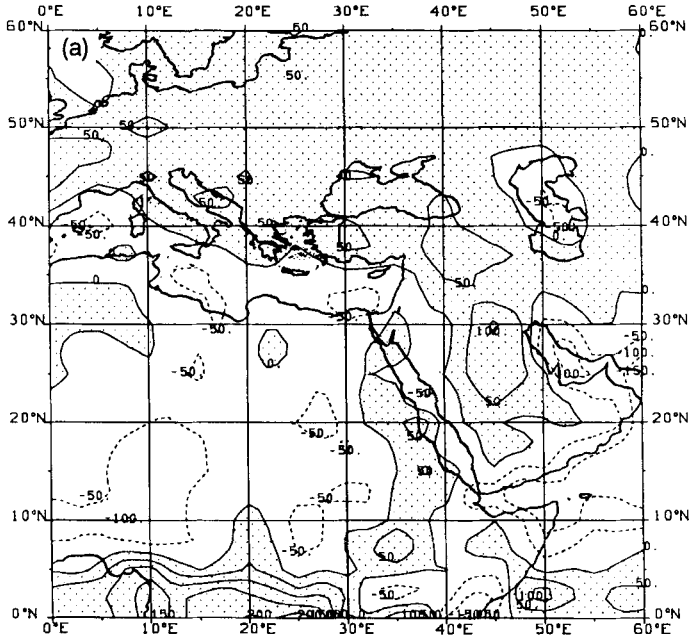

Figure 2. As in Fig. 1, but for the moisture budget, Eq. (7).

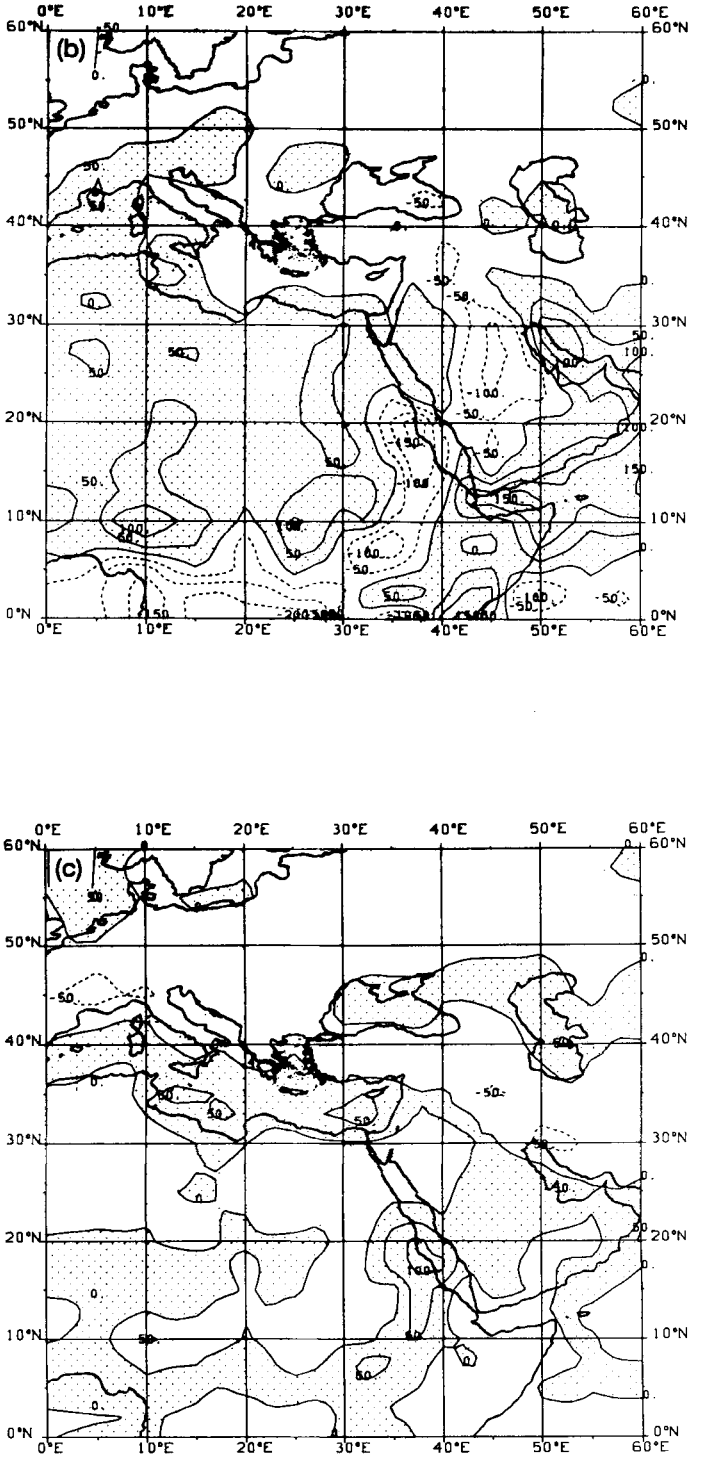

Figure 2. Continued.

high, and are explained by the errors in the calculation of the horizontal fluxes in proximity to the northern boundary.

Results resemble those of earlier studies by Kasahara *et al.* (1987), Chen and Baker (1986), Mizzi and Kasahara (1989), Hoskins *et al.* (1989), although these studies were in general for shorter periods and incorporated major smoothing in order to keep the more reliable larger-scale features. Here, the averaging period is relatively long (18 months spread equally over 6 years) and some finer scales show up. For example, Fig. 3 shows the vertically-integrated diabatic heating up to 50 hPa for an average winter from the global 1979–89 ECMWF analyses, following Hoskins *et al.* (1989).

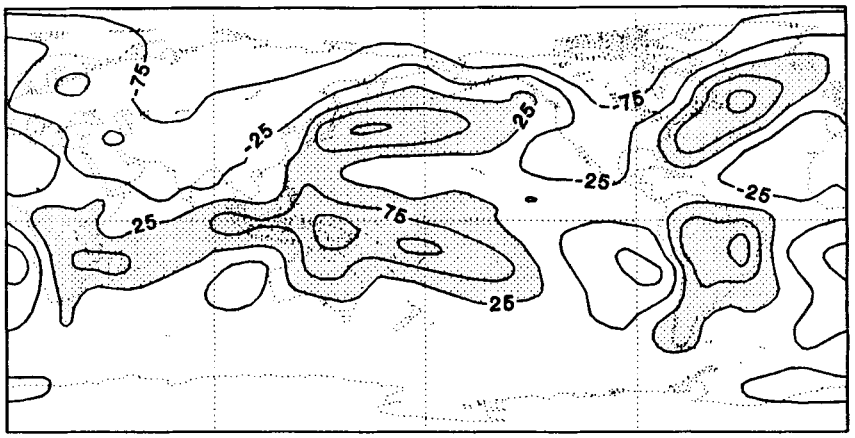

Figure 3. Global horizontal distribution of the vertically integrated (surface to 50 hPa) diabatic heating for Dec.–Feb. data for the period 1979–89; from Hoskins *et al.* (1989) with 5×5 degrees horizontal resolution.

The agreement with Fig. 1(a) is quite good in the tropics although the maxima in Fig. 3 are about half the value, probably because of the lower resolution of 5×5 degrees and the enhanced smoothing. However, a narrow band of diabatic heating tending to be positive in Fig. 3 connects the tropics with the north Atlantic through the Mediterranean and corresponds well in the present study with the relatively large positive values over the Mediterranean (Fig. 1(a)).

In order to understand the interaction between the different terms in the thermodynamic equation, Figs. 1(b) and 1(c) show the contributions due to the steady-state term ($[HA_T^0]_p + [VM_T^0]_p$) and the transient term ($[HA_T^1]_p + [VM_T^1]_p$) in Eq. (6) respectively. Since the storage term is negligible for the long averaging period (18 winter months) the sum of the terms in Figs. 1(a, b and c) vanishes. In the steady-state terms, Fig. 1(b), one can notice the tropical cooling due to the ascending motion, and northward at 10–30°N latitudes the warming due to subsidence of the downward branch of the Hadley cell. The Mediterranean region is typified by large cooling centres—particularly in the cyclogenetic regions—caused by the steady-state motion. This means that the steady-state flow removes energy formed by diabatic processes in these regions (compare Figs. 1(a) and 1(b)). The transient-term contribution representing the effect of the cyclone motion (Fig. 1(c)) is in general negligible south of 30°N. In the North Sea there is a transient cooling which is mainly balanced by the steady-state advection. Such a balance is typical for a baroclinic region in which the basic flow transports energy to the perturbations and the perturbations transport the energy further to the cold continent, as shown by the heating over Europe in Fig. 1(c). The balance in the Mediterranean,

however, is just in the opposite sense since there is a significant diabatic heating associated with a cooling by the steady-state motion, and a warming by the transients. Hence, the processes in the Mediterranean, and in particular those related to cyclone dynamics, are more of a tropical nature than those of the baroclinic lows in the mid latitudes; see also the further comparison of vertical profiles in section 4(c).

Figures 2(a, b and c) show the winter-averaged moisture balance terms in Eq. (7). The moisture net sink $[\overline{H}_q]_p$ in Fig. 2(a) represents the tropical rain, in close agreement with Fig. 1(a) and also with the observed rainfall. For instance, at the station Eala Congo (0°N, 18°E) the average winter rainfall (Dec.–Jan.–Feb.) is 373 mm (349 mm for evaporation), following Bultot and Griffiths (1972, p. 291), whereas the calculated net sink $[\overline{H}_q]_p$ from Fig. 1(a) at the nearest gridpoint (0°N, 17.5°E) is 181 W m^{-2} corresponding to 570 mm (Eq. (12)). The total vertical transport ($[VM_q^0]_p + [VM_q^1]_p$) at this gridpoint is 178 W m^{-2} (560 mm), nearly equalling the moisture net sink. The difference between the calculated and the observed values is about 40–50% which is as expected for the present residual method (see Appendix 2). The integrated diabatic heating at the same gridpoint is 139 W m^{-2} (437 mm) which is 20% lower than the net condensation. This is explained either by the radiative cooling or alternatively by the more accurate ECMWF temperature analysis as compared to that of moisture (Trenberth and Olson 1988). At the same tropical location, Hoskins *et al.* (1989) obtained a diabatic heating value of 50 W m^{-2} that is too low compared with the observations (Fig. 3).

Over Europe, the calculated net condensation is about 50 W m^{-2} (160 mm), with a maximum in the west, which is in good agreement with the climatological rainfall distribution in winter (Wallen 1970). In Paris, for instance, the average observed rainfall for the period December to February is 146 mm. As expected, over water areas the evaporation dominates. Over the subtropical deserts there is a weak net source contributed by the levels above 850 hPa probably resulting from evaporating clouds. Over the Arabian Peninsula, however, we find a clear maximum of net condensation of 109 W m^{-2} at position 30°N, 45°E. This paradox of the dry desert with nearly zero rainfall being a net condensation region is explained by significant condensation in medium-level and high-level clouds—maximum condensation of 25×10^{-3} W kg^{-1} at 550 hPa. The moisture is carried by horizontal advection to the Arabian Peninsula by the steady-state motion, Fig. 2(b), and the condensed cloud water leaves the region by advection and not through rainfall (Alpert and Shay-El 1991).

In Fig. 2(b) the following major features of the steady moisture terms are noticed. Firstly, the strong moisture convergence by the vertical motion in the tropics extending up to about 8°N. Secondly, the moisture divergence (drying) in the desert band due to subsidence dominating the 200–850 hPa layer (see section 4(b)). A very interesting feature is the narrow band of steady-state horizontal advection of moisture up to 300 hPa from the tropics north-eastward to the Arabian Peninsula, which is associated with the quite steady flow of the subtropical jetstream. In the transients' contribution, Fig. 2(c), it appears that the Mediterranean, along with other seas, constitutes a moisture source for the travelling cyclones.

(*b*) *Vertical profiles: comparison with the tropics and other regions*

Figure 4 shows the vertical cross-section of the diabatic heating, $\overline{H}_T$, along 30°E longitude, which crosses the eastern Mediterranean. One can see the diabatic heating in the tropical region extending up to 250 hPa. At mid troposphere the radiative cooling dominates. As one moves northward from the tropics the convective processes weaken while the sensible heat flux strengthens but is mainly restricted to the planetary boundary

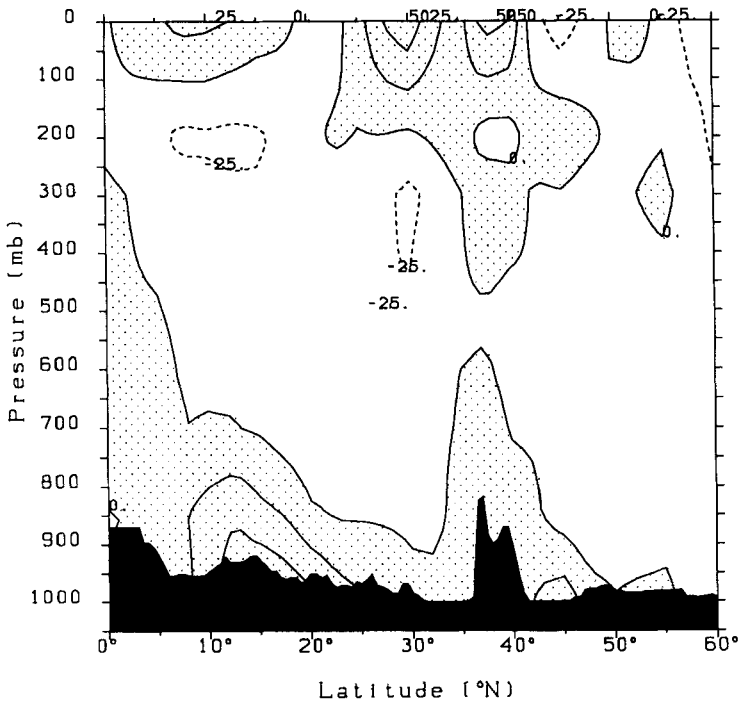

Figure 4. Vertical cross-section of the diabatic heating, $\overline{H}_T$, along 30°E longitude for an average winter (Dec.–Feb.) based on 1982–88 ECMWF data. Positive (solid) and negative (dashed) contours are at intervals of 25×10^{-3} W kg^{-1}. Positive-value regions are shaded. Topography is drawn in black at the bottom.

layer. The resulting integrated diabatic heating $[\overline{H}_T]_p$ in the subtropics is therefore negative (Fig. 1(a)). This diabatic cooling over the Sahara was conjectured much earlier by Charney (1975). Above the Mediterranean and the Anatolian Heights the convective boundary layer again deepens and also the intrusion of the stratospheric heating intensifies between 25 and 55°N as mentioned earlier, and even penetrates the 500 hPa level over Turkey (38°N). Over Europe, north to the Black Sea (approx. 45°N), the continent becomes relatively cold and dry, thus leading to the dominance of the radiational cooling throughout the troposphere.

In order to compare the relative contribution of each term in Eqs. (6) and (7) separately, we show in Figs. 5(a, b, c) and 6(a, b, c), the vertical profiles of these terms at three selected gridpoints. The first point at position 35°N, 30°E represents the eastern Mediterranean in Figs. 5(a) and 6(a); the second, the tropical point of maximum diabatic heating at position 0°N, 20°E is shown in Figs. 5(b) and 6(b) and the third point represents the cyclogenetic region of the North Sea, 57.5°N, 5°E, in Figs. 5(c) and 6(c). The storage terms S_T, S_q are negligible at all points because of the long averaging period.

In the tropical profiles (Figs. 5(b) and 6(b)) the balance is mainly between the diabatic heating, $\overline{H}_T$, which is basically latent heat and the adiabatic cooling due to the steady vertical motion VM_T^0. Similarly the moisture balance is between the steady vertical transport, VM_q^0, and the net condensation (sink), $\overline{H}_q$. This corresponds well to results obtained also by scale analysis in the tropics as for example (Holton 1979, Eq. 12.11)

$$\omega S \cong H_T/c_p \tag{13}$$

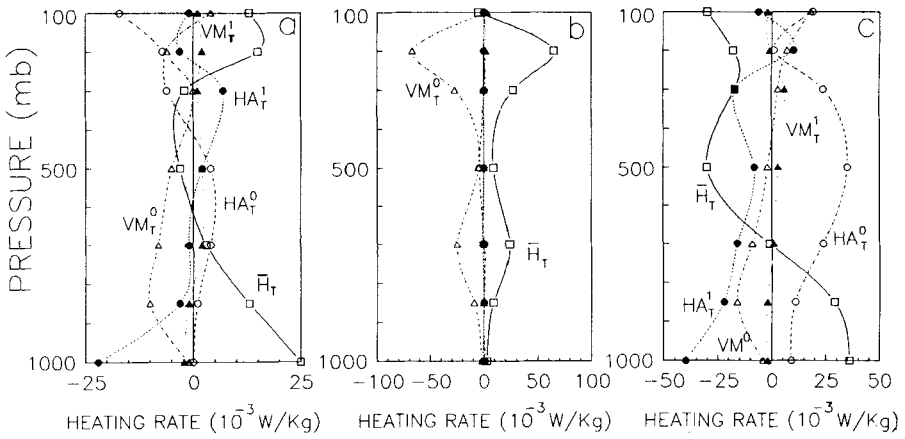

Figure 5. Vertical profiles of diabatic heating, $\bar{H}_T$, (—□—□—□—); steady horizontal advection, HA_T^0, (○- - -○- - -○); steady vertical motion, VM_T^0, (△- · -△- · -△); transient horizontal advection, HA_T^1, (●- - - ●- - - ●); transient vertical motion, VM_T^1, (▲ · · · · ▲ · · · · ▲), for average winter (Dec.–Feb.) at three selected gridpoints as follows: (a) 35°N, 30°E, in the eastern Mediterranean; (b) 0°N, 20°E in the tropics; (c) 57.5°N, 5°E in the North Sea—based on 1982–88 ECMWF data. Notice the very different heating scales for the three regions. For further detail see Eq. (6) and text. Points A, B and C are as shown in Fig. 1(c).

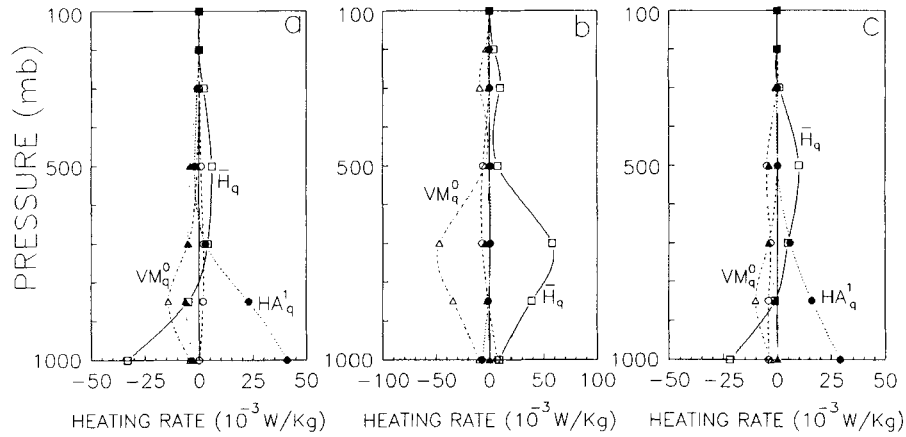

Figure 6. As in Fig. 5, but for the moisture balance terms in Eq. (7).

where $S = (p/p_0)^\kappa \partial\theta/\partial p$ is the static stability parameter and the diabatic heating H_T is due to latent heat release.

The two maxima appearing in the diabatic-heating profile in the tropics are similar to reports by Yanai *et al.* (1973), and Chen and Baker (1986). Weare (1988) shows by applying the UCLA GCM model that this two-maxima profile is the result of superposing a cumulus heating profile with a 600 hPa maximum on a second profile due to the large-scale precipitation that has two maxima (at 600 and 200 hPa). There is a significant difference between the $\bar{H}_T$ and $\bar{H}_q$ profiles. The net condensation tends to maximize in the lower troposphere (700 hPa) while the $\bar{H}_T$ maximum is in the higher troposphere (200 hPa). This difference is explained through the convection process. The cumulus cells transport the moisture from the lower to the upper levels where the latent heat is

released. The difference between the two profiles can be used to estimate the total turbulent heat transfer in convective clouds (Yanai *et al.* 1973).

The North Sea balances are more complex. The heat balance (Fig. 5(c)) shows that the steady warm horizontal advection, HA_T^0, dominates and reaches a maximum at 500 hPa. The moisture balance in Fig. 6(c) shows a net moisture source up to 800 hPa, probably due to the sea moisture fluxes. The terms HA_q^0, VM_q^0, and VM_q^1 transfer moisture to the region while HA_q^1 removes the moisture with a maximum near the surface. These balances correspond to the influence of cyclones which remove the excess energy (and moisture) supplied by the steady flow and the heat fluxes.

The heat balance in the Mediterranean (Fig. 5(a)) looks like a composite of those in the North Sea and the tropics. The diabatic heating profile, $\overline{H}_T$, is similar to that in the North Sea except that an additional 200 hPa maximum exists due to the stratospheric warming. The horizontal steady advection, HA_T^0, does warm the lower troposphere and cool the higher troposphere as in the North Sea but values are significantly lower in the Mediterranean. In contrast to the North Sea and like the tropics, the dominant cooling term is the steady adiabatic cooling, VM_T^0, with a maximum at 850 hPa. The transient horizontal advection HA_T^1, which is the primary cooling term in the North Sea, cools the lower troposphere in the Mediterranean and warms the higher levels.

The moisture balance (Fig. 6(a)) is very similar to that for the North Sea (Fig. 6(c)) except in the following aspects. Firstly, the moisture source, $-\overline{H}_q$, near the surface, reflecting the sea fluxes, is higher. Secondly, the steady vertical transport, VM_q^0, is stronger, probably reflecting the more tropical tendency of the eastern Mediterranean region. Thirdly, the transient moisture advection, HA_q^1, is stronger.

To summarize, the Mediterranean is characterized by prominent steady-state contributions just as in the more southern tropical region, but contrary to the tropics the transient contributions in the Mediterranean related mainly to the cyclone activity are not at all negligible. As happens in the case of the North Sea, the transients do remove considerable heat and moisture from the Mediterranean. The vertical profiles of the residuals $\overline{H}_T$, $\overline{H}_q$, show mainly the sea influence, i.e. heat and moisture subscale fluxes, but there is no prominent influence of the latent heat release.

5. Diabatic heating/net condensation for a composite Cyprus low

In the preceding section we studied the average winter characteristics of the diabatic heating and net condensation in the Mediterranean. Since the Cyprus low is the principal agent of cyclonic activity in the eastern Mediterranean during winter, the present section focuses only on these synoptic situations in which the lows are centred over a certain region around Cyprus; then we repeat the residual analysis for calculating the diabatic heating and net condensation. This is performed for the different sectors of the composite cyclone.

(*a*) *The composite Cyprus low*

In order to obtain a representative selection of Cyprus lows, four selective criteria have been applied for the six winters, twice a day. These criteria are:

(i) Winter season, i.e. December to February.
(ii) The 1000 hPa minimum defined as the low centre was located within the geographic rectangle of 31–39°E longitude and 32–38°N latitude (Fig. 7).
(iii) The 1000 hPa geopotential height at the cyclone centre was less than 100 m. This is equivalent to a surface pressure at m.s.l. height of about 1010 hPa.

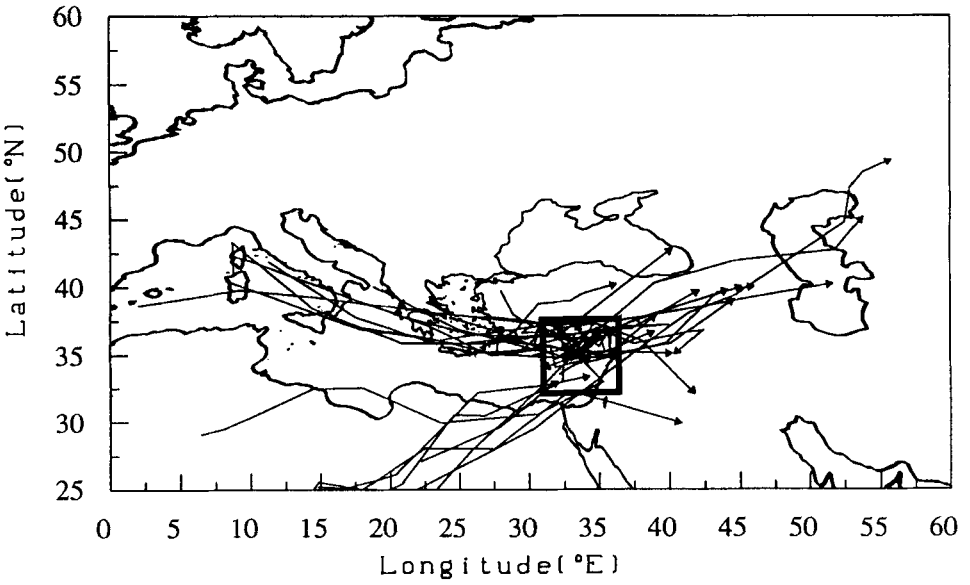

Figure 7. Cyclone tracks for which the composite Cyprus low was defined. These tracks were selected out of the 1982–88 ECMWF data-set based on the four criteria detailed in the text. The geographic rectangle of 31–39°E longitude and 32–38°N latitude referred to in the aforementioned criteria is designated by a heavy line.

(iv) The cyclone was identified in at least three consecutive ECMWF data-sets. That means that its lifetime was longer than 24 hours. Further details about the selection method and track definition are found in Alpert *et al.* (1990a).

Figure 7 shows the cyclone tracks identified by this method. There are two major routes, one along the northern Mediterranean primarily during the period December to January, and the southern route along the North African coast, typical for February, Alpert *et al.* (1990b).

The first three criteria led to 92 situations which then dropped to 67 when the fourth criterion was applied. The number of cyclones left was 35, so each cyclone stayed, on the average, in the aforementioned rectangle for more than 12 hours ($67/35 \approx 2$ data-sets). The average geopotential height at the cyclone centre was 49 m (approx. 1005 hPa). Regarding the development status of these situations, most (37 cases) were found to be in their mature state. Only twelve were identified as developing, and the rest (18 cases) as decaying. Hence, the composite low can be regarded as representing primarily the mature state but the presence of a mixture of all three phases presumably tends to emphasize the effects of local topographical forcing. In the 12 hours preceding the cyclone identification, the average deepening rate was -1.5 m/12 h but this changed later to a much larger filling rate of $+13$ m/12 h.

The region was found to be cyclogenetic in the sense that cyclones tended to stay longer there (Alpert *et al.* 1990a). In the current selection of cyclones the average speed of a cyclone along its track was 8.4 m s^{-1} while over the eastern Mediterranean rectangle in Fig. 7, they slowed down to an average speed of 4.9 m s^{-1}.

The main synoptic features of the composite cyclone are shown in Figs. 8(a–f). The 1000 hPa geopotential map (Fig. 8(a)) shows the cyclone centre over Cyprus. It is interesting to note the association of the average Cyprus low with a deep cyclone over the North Atlantic along with a blocking anticyclone over western Europe and northern

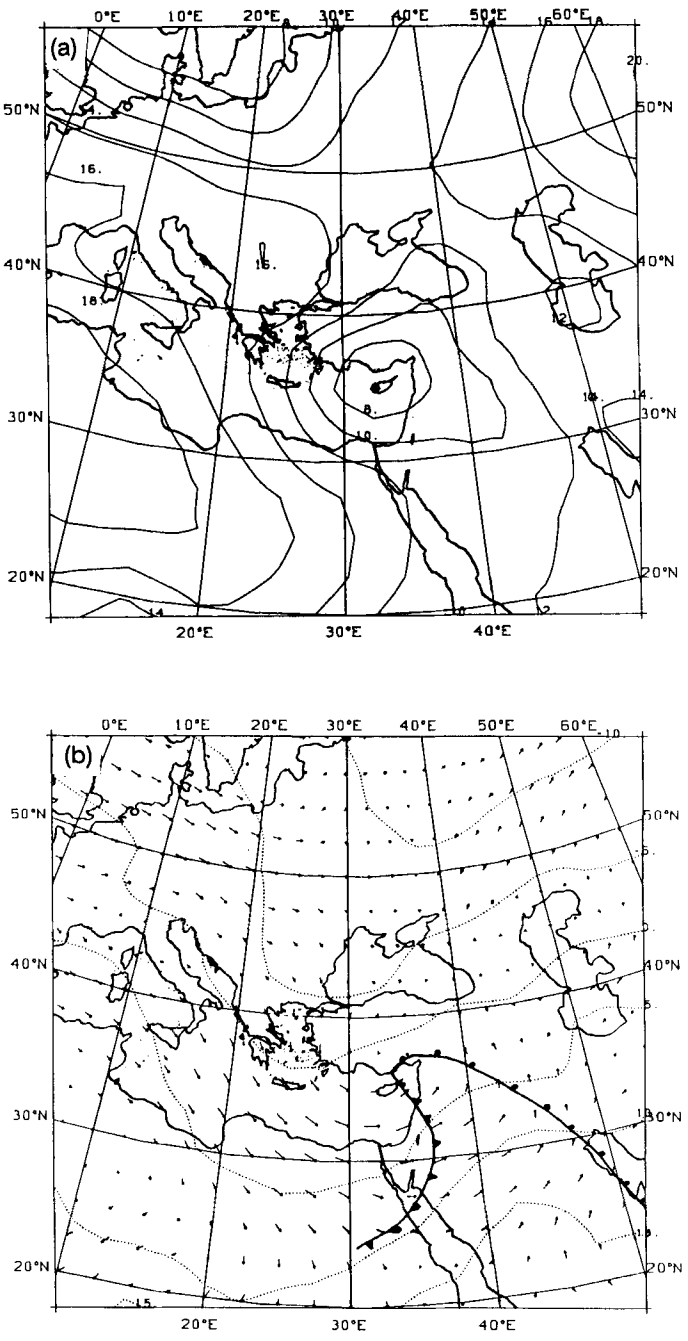

Figure 8. Main charts for the composite Cyprus low as follows: (a) 1000 hPa geopotential height (2 dam interval); (b) 850 hPa temperature (dotted, 5 K interval) and wind vector arrows representing 6-hour displacements; (c) 850 hPa rate of temperature advection with a 25×10^{-3} W kg^{-1} interval. Positive (solid) and negative (dashed) contours where positive-value regions are shaded; (d) 850 hPa geopotential height (solid, 3 dam interval) and relative humidity (dotted, 10% interval); (e) 500 hPa geopotential height (solid, 3 dam interval) and vertical p-velocity (dashed, 5×10^{-2} Pa s^{-1} interval, negative values shaded); (f) 200 hPa isotachs (10 m s^{-1} interval; values exceeding 50 m s^{-1} shaded) and 3-hour displacement wind arrows. The cold and warm fronts in (b) were plotted along the lines of maximum advection rate in (c).

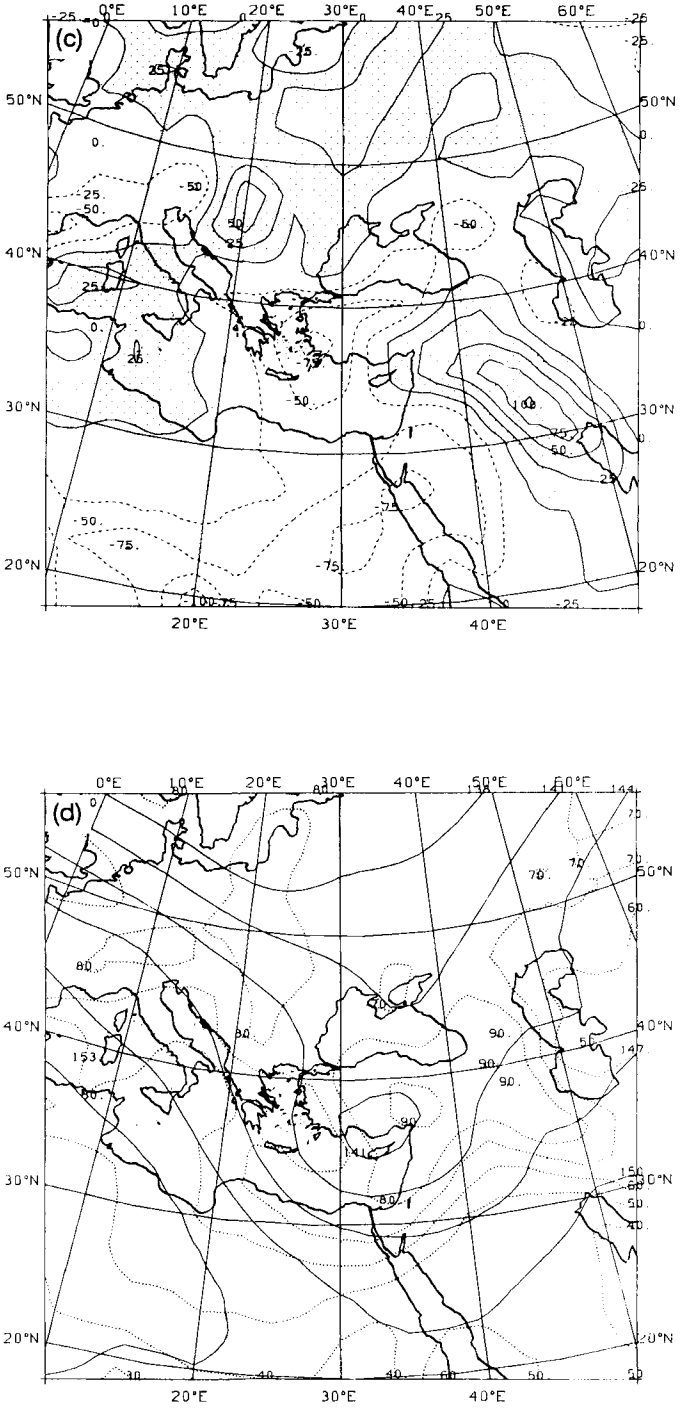

Figure 8. Continued.

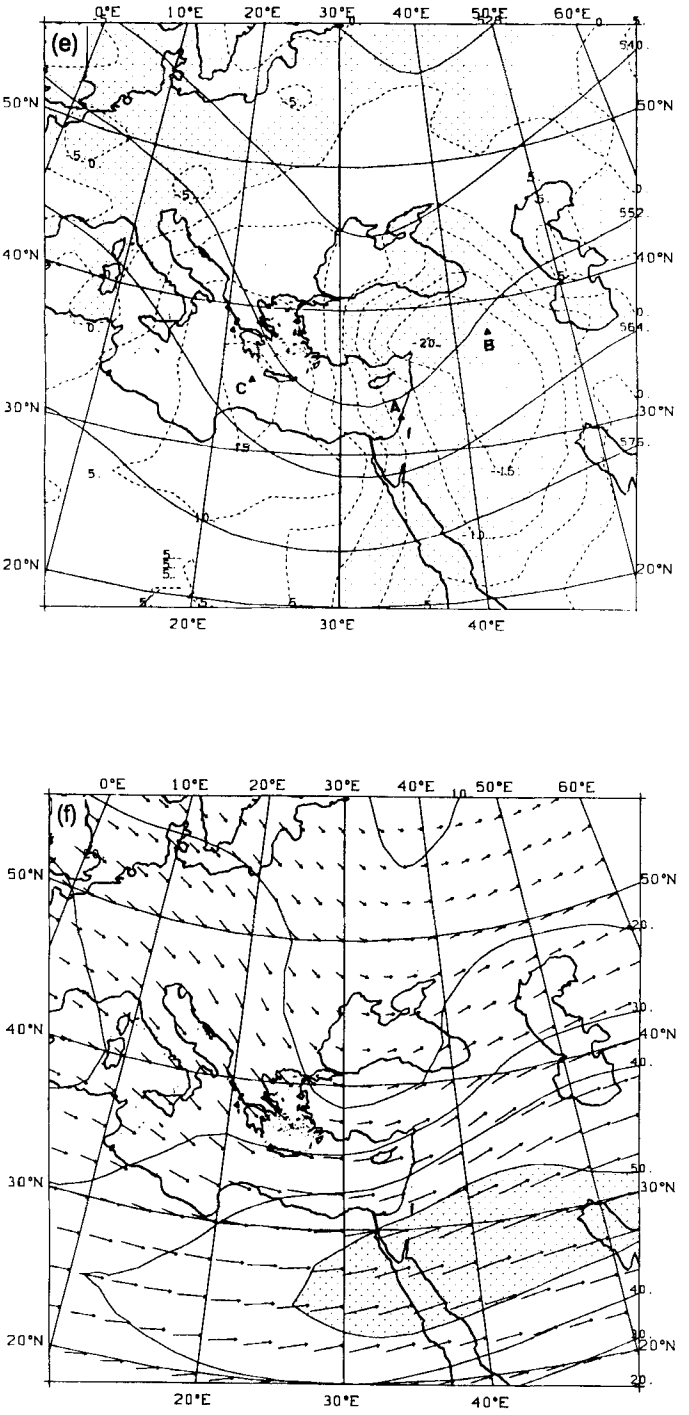

Figure 8. Continued.

Africa. This fits well with the classical description of a Cyprus low (H.M.S.O. 1962; Kallos and Metaxas 1980). Figure 8(b) presents the 850 hPa isotherms (dotted) and wind arrows, and although 67 data-sets have been averaged, fronts can still be clearly identified. The warm and cold fronts were drawn where the 850 hPa maximum warm and cold advections, respectively, were found (Fig. 8(c)). A secondary maximum of cold advection could also be noticed (Fig. 8(c)) from the Black Sea to the south-western coast of Turkey and the Island of Rhodes at a position 37.5°N, 27.5°E: it will be referred to later. Figure 8(d) shows the 850 hPa height (full) and relative humidity (dotted). The moisture distribution follows the frontal structure with a 90% maximum ahead of the warm front and an 80% maximum in the wake of the cold front. The higher-level flow at 500 hPa (Fig. 8(e)) is illustrated by the height field along with the vertical velocity, ω, where upward motion is shaded. The structure closely fits the quasi-geostrophic theory for a baroclinic low with upward motion east of the trough and downward motion to the west. The trough, however, is only slightly to the west of the centre of the surface low, leading to only a very slight tilting with height. The nearly barotropic nature is also probably associated with the averaging, and may not be representative of a Cyprus low. The 200 hPa wind isotachs with shading over 50 m s^{-1} (Fig. 8(f)) show that the cyclone is found at the cyclonic (northern) side of a very strong jetstream. Considering the fact that this is an averaged map, the relatively high wind intensity indicates that a strong relation may exist between Cyprus-low activity and the jetstream at 29 to 30°N latitudes. In Fig. 8(e) three points of interest in the vertical profiles are shown and will be used in the discussion later. Point A, at position 32.5°N, 35°E, is right in the active convective region of the cold front, point B, at position 37.5°N, 42.5°E, is at the upward-flow region over the warm surface front, and Point C, at position 35°N, 22.5°E, is right in the centre of the downward-motion region west of the cyclone region.

Next, sections 5(b, c, d) will discuss the diabatic heating and the net condensation for the composite Cyprus low, while section 5(e) will compare these with distributions for a single low on 6 January 1987.

(*b*) *Horizontal distributions of diabatic heating and net condensation*

The distributions of vertically integrated diabatic heating and net condensation for the composite Cyprus low are shown in Fig. 9(a, b). As expected, values here are much larger than those of the total winter averages (Figs. 1(a) and 2(a) respectively), and there are important differences. In Fig. 9(a) two major diabatic heating maxima of 346 and 244 W m^{-2} appear at the warm and cold fronts respectively. At the high region west of the cyclone the radiative cooling dominates (-250 W m^{-2} over western Greece). The net condensation also indicates a major maximum of heating of 329 W m^{-2} along the warm front. Above the sea the strong turbulent sea surface fluxes result in a net moisture source maximum of -337 W m^{-2}. This probably weakens the cold front maximum owing to the release of convective latent heat along the coast, but a maximum line could still be noticed. To estimate the sea-surface turbulent fluxes, Figs. 10(a, b) show the distributions of the diabatic heating and net condensation for the lowest level at 1000 hPa. The strongest fluxes are in the lee of the western Turkish mountains because of the marked contrast between the cold, dry north-easterly winds (Figs. 8(a, b)) and the relatively warm sea. Through a bulk parametrization the resulting planetary boundary-layer fluxes over the sea can be estimated by:

$$F_T = c_p \rho C_T |\mathbf{V}| (T_w - T_a) \tag{14}$$

$$F_q = L \rho C_q |\mathbf{V}| (q_w - q_a) \tag{15}$$

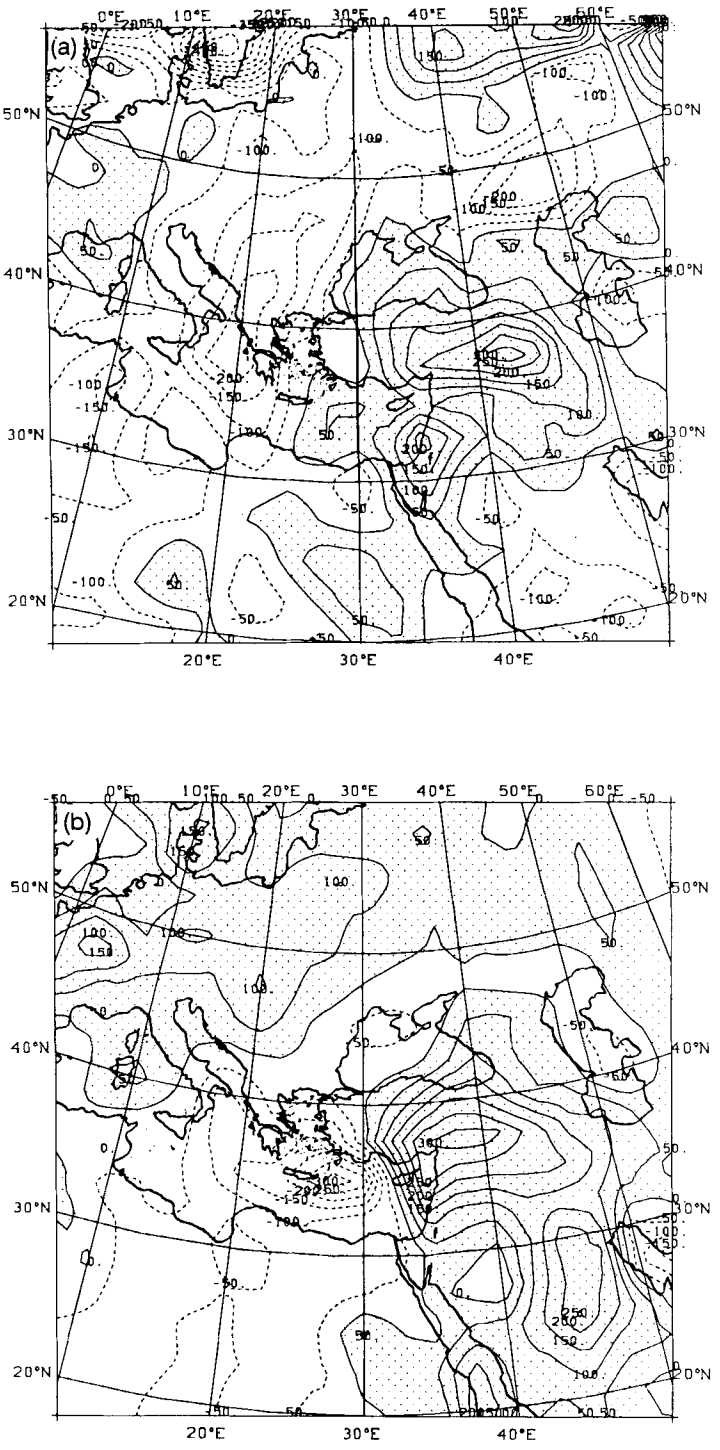

Figure 9. Distributions of vertically integrated: (a) diabatic heating, $[H_T]_p$; (b) net condensation, $[H_q]_p$—for the composite Cyprus low, based on 1982–88 ECMWF analyses. Positive (solid) and negative (dashed) contours are plotted at intervals of 50 W m^{-2}. Positive value regions are shaded.

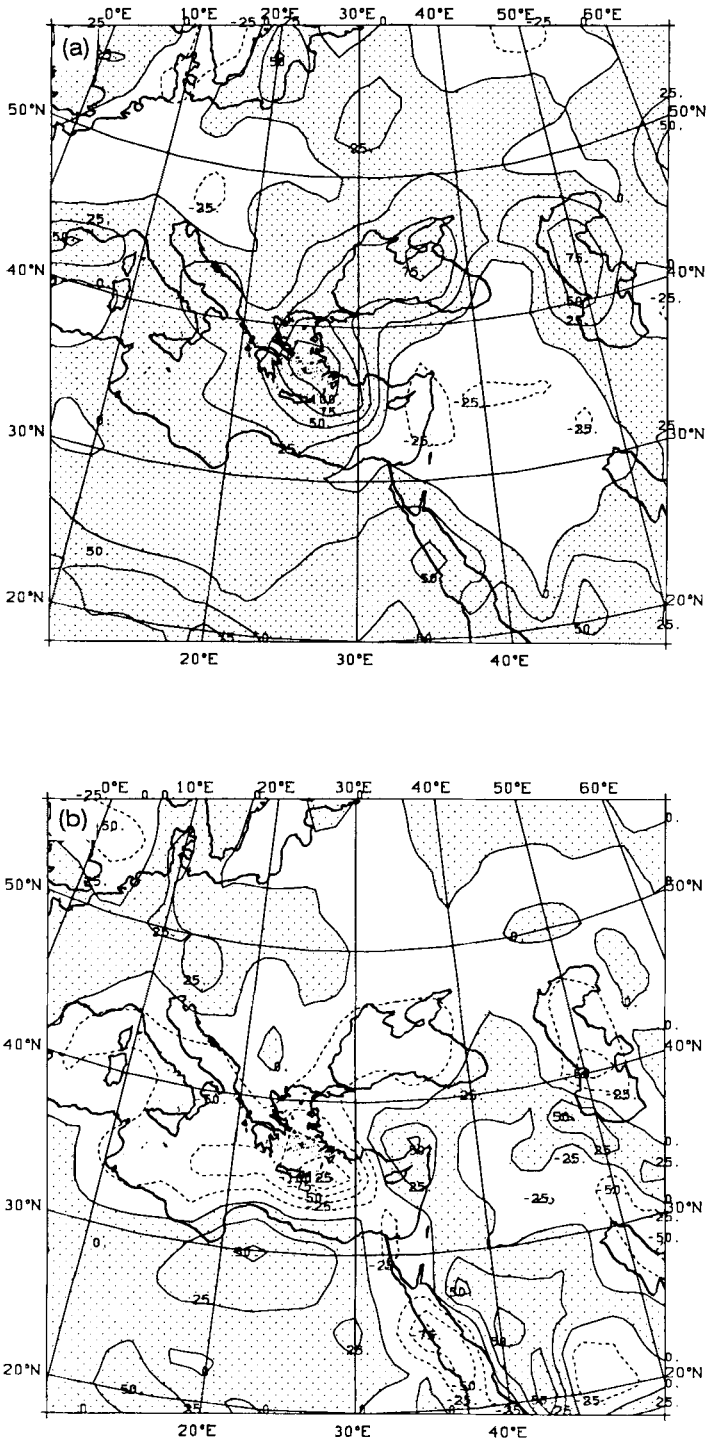

Figure 10. As in Fig. 9(a, b) but for the 1000 hPa surface with a 25×10^{-3} W kg^{-1} interval.

where $C_T = 1.4\times10^{-3}$, $C_q = 1.6\times10^{-3}$, following Krishnamurti *et al.* (1987). The given field values at the point where the maximum fluxes were calculated, i.e. points 35°N, 27.5°E, are: $q_a = 0.0063$, $T_w = 17.3$ °C, $T_a = 13.0$ °C, $|\mathbf{V}| = 10.6$ m s^{-1}, $q_w = 0.0123$ where the 1000 hPa level represents the lowest atmospheric level indexed by subscript 'a'. Equations (14) and (15) then lead to $F_T = 77$ W m^{-2}, $F_q = 305$ W m^{-2}. The corresponding integrated values from Figs. 9(a, b) are $[H_T]_p = 49$ W m^{-2}, $[H_q]_p = 337$ W m^{-2}. The reason for $[H_T]_p$ being smaller than F_T is mainly because of the radiative cooling contribution.

(*c*) *Vertical cross-sections and profiles*

The vertical variations of H_T and H_q along the convective region of the cold front in the eastern Mediterranean (along 35°E) are shown in Fig. 11(a, b). The good agreement between H_T and H_q over the Mediterranean and the Turkish mountains supports the suggestion that the diabatic heating is primarily due to latent heat release although there are important differences in the vertical variation to be discussed later. A second convective cell is situated in the tropics (7.5°N) and an additional higher troposphere maximum of diabatic heating is found in proximity to the jetstream.

A latitudinal vertical cross-section along 37.5°N illustrates, in Fig. 12, the vertical variation of various terms in the thermodynamic equation, basically representing a baroclinic low. East of the 500 hPa trough, at ~30°E, a warm sector along with warm advection through the full troposphere (Fig. 12(a)) and adiabatic cooling (Fig. 12(b)) exist, while west of the trough cold advection along with adiabatic heating prevails. But the two terms do not balance each other exactly and Fig. 12(c) shows the diabatic heating required to keep the thermodynamic energy nearly in balance. The diabatic heating increases with latitude, tilting towards the warm sector with a maximum above the Kurdistan mountains (45°E). As will be shown later, this is associated with latent heat release at the warm front. Above the Aegean Sea (25°E) one can notice the sensible heat flux up to 800 hPa. In the cold sector, a maximum of diabatic cooling at 300 hPa exists. This could result from radiative cooling but the symmetry of this sector with the warm sector in the high troposphere lends support to the possibility that the calculated vertical winds in the higher troposphere and the associated adiabatic cooling or heating may be slightly exaggerated by the ECMWF analysis (see also Mizzi and Kasahara 1989).

The storage term (Fig. 12(d)) shows that the warm sector cools and the cold sector warms. Two other interesting features should be noted in the horizontal advection term distribution, HA_T, in Fig. 12(a). Firstly, the vertical variation presents two maxima, one near the surface and the other near the tropopause. This is in agreement with the two vorticity maxima found by Alpert *et al.* (1990a) in the vertical variation, and also supports the idea that two different cyclogenetic mechanisms are important in the eastern Mediterranean: surface processes and the subtropical jetstream,* Alpert and Warner (1986). Secondly, the major horizontal gradient of advection over the western slopes of the Turkish mountains probably indicates that the cold northerly air turns around the mountains (El Fandy 1946).

To complement the picture along the 37.5°N vertical cross-section, Fig. 13(a–d) presents the corresponding terms in the moisture balance through the composite Cyprus low. Figure 13(a) shows moisture convergence in the warm sector up to about 500 hPa, and moisture divergence above the sea, west of 27.5°E, where the sea fluxes maximize. The residual term—net condensation—in Fig. 13(c) shows the strong latent heating in the warm sector in agreement with the diabatic heating residual in Fig. 12(c). In the

* A similar linkage of the lower baroclinic region to the upper jet was also indicated in the October 1987 storm over S. England, e.g. Hoskins and Berrisford (1988).

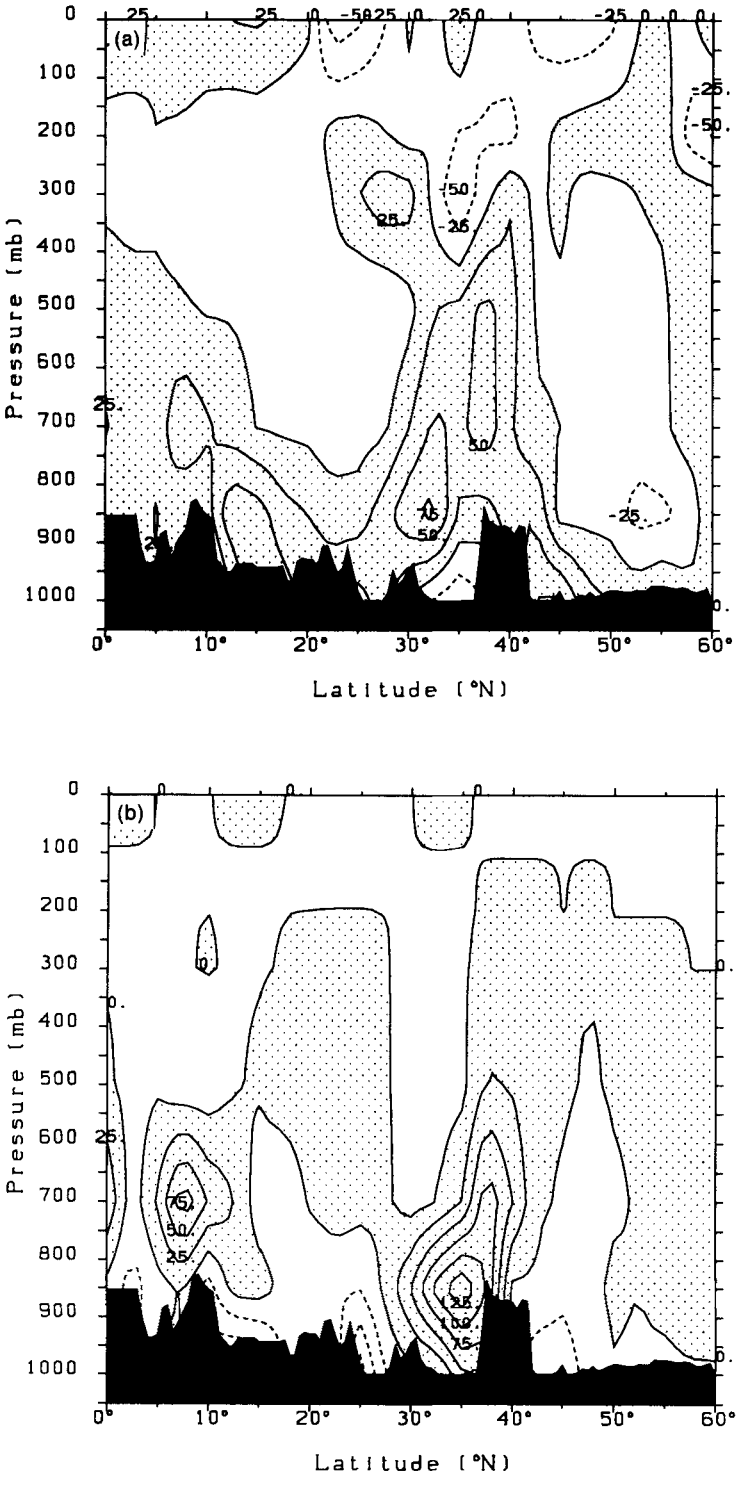

Figure 11. Vertical cross-sections of: (a) the diabatic heating, H_T; (b) the net condensation, H_q, along 35°E longitude for the composite Cyprus low. Positive (solid) and negative (dashed) contours are at intervals of 25×10^{-3} W kg^{-1}. Positive-value regions are shaded.

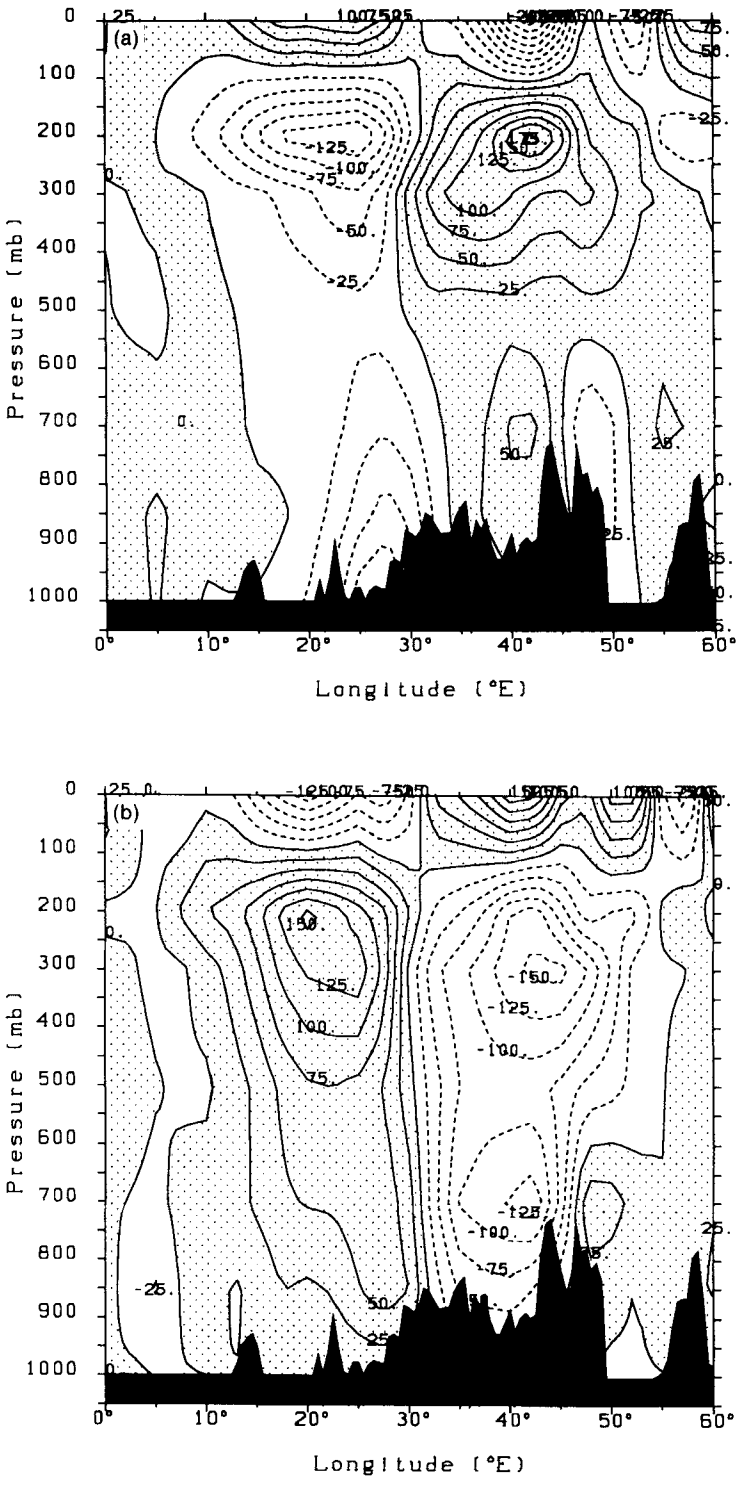

Figure 12. Vertical cross-sections along 37.5°N latitude for a composite Cyprus low of: (a) horizontal advection term, HA_T; (b) the vertical motion term, VM_T; (c) the diabatic heating, H_T; (d) the storage term, S_T—based on 1982–88 ECMWF analyses. Contours and shading as in Fig. 11.

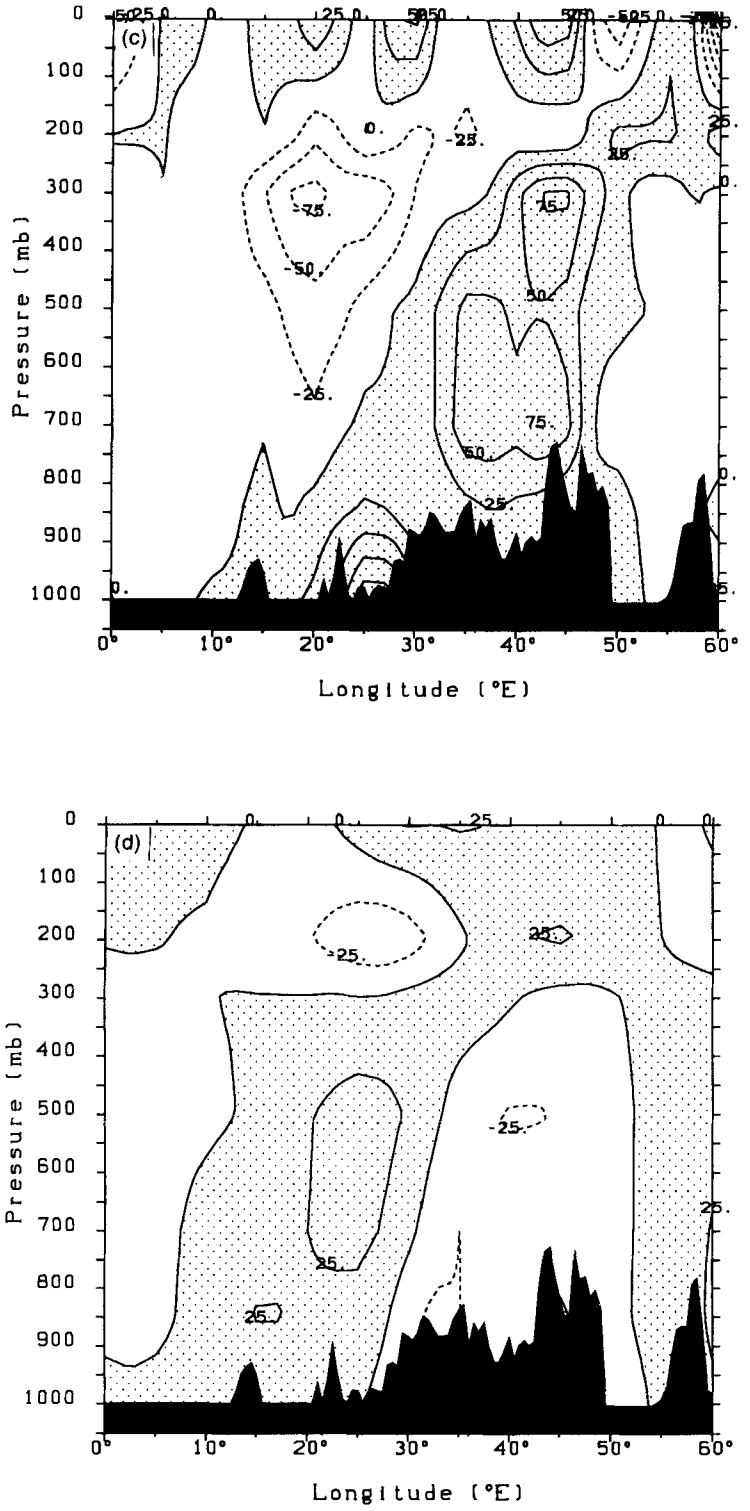

Figure 12. Continued.

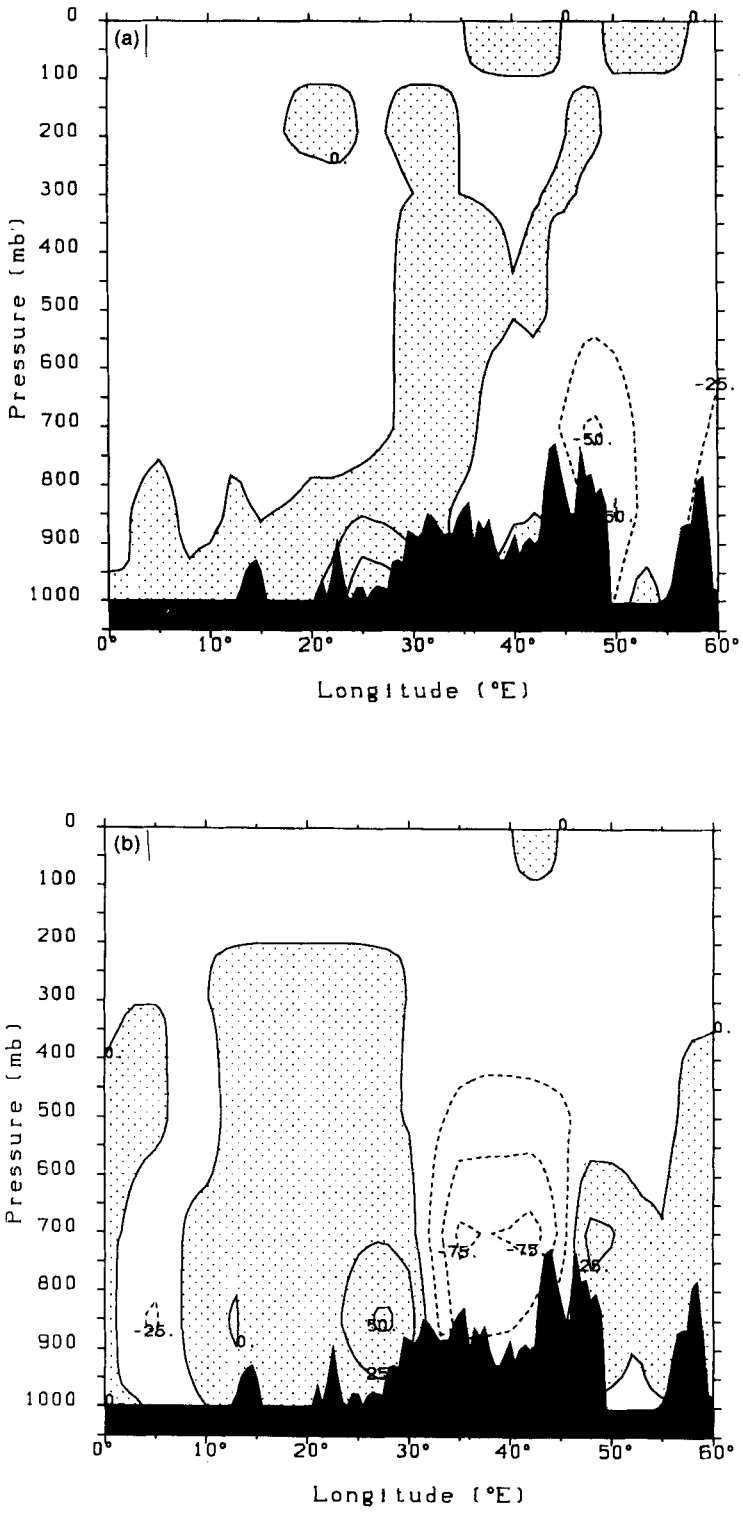

Figure 13. As in Fig. 12(a–d), but for the moisture budget terms.

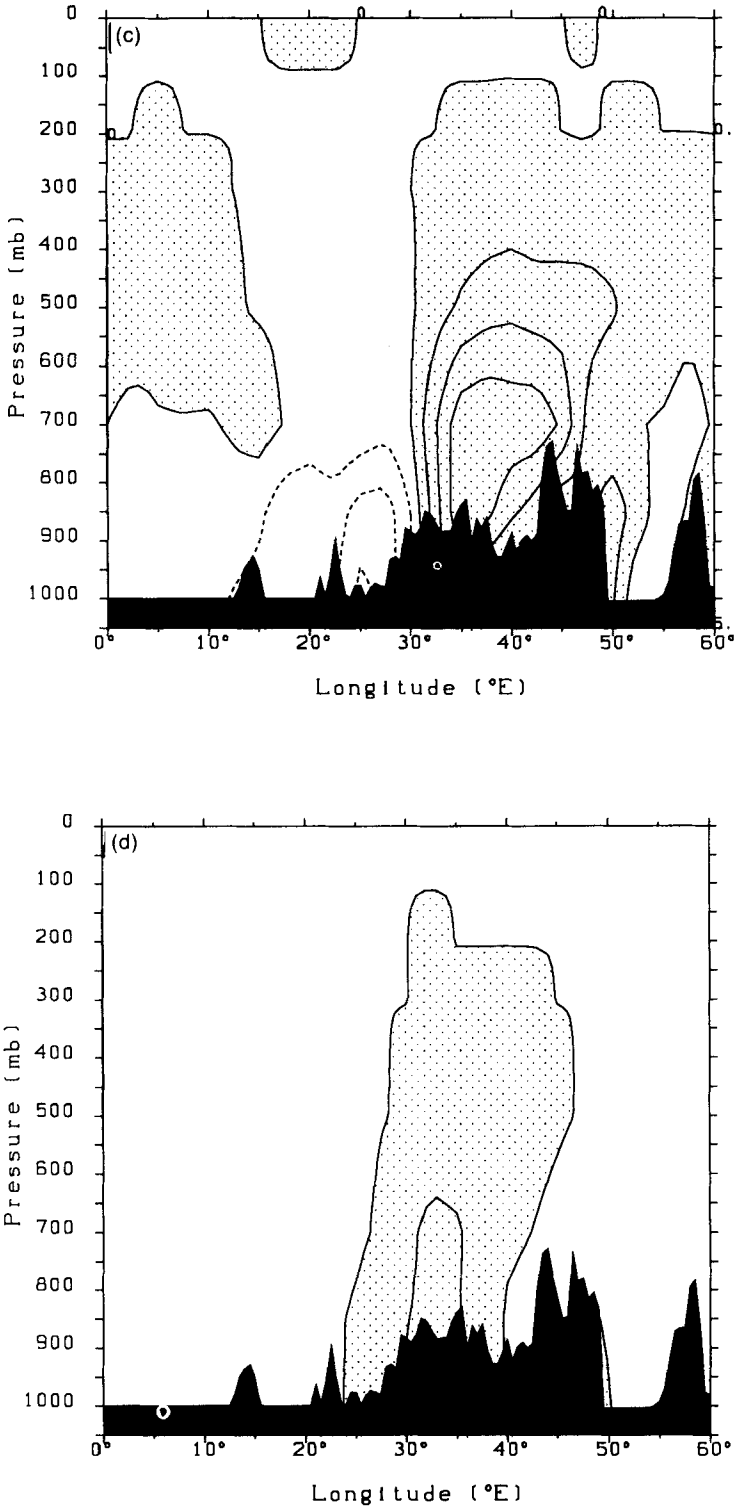

Figure 13. Continued.

downward cold sector the sea surface fluxes moisten the atmosphere up to about 700 hPa. The storage term (Fig. 13(d)) shows that the only variation with time is loss of moisture in the warm sector and moisture gain in the cold sector, corresponding to the thermal processes (Fig. 12(d)).

The vertical profiles of the heating and moisture terms (Figs. 14(a), 15(a) respectively) right in the centre of the convective region (point A in Fig. 8(e)) indicate the latent heating released by the cumulus convection. The diabatic heating has a wide 850 hPa maximum of 84×10^{-3} W kg^{-1} (7 K d^{-1}) as compared to a larger and narrower net condensation maximum of 113×10^{-3} W kg^{-1}. As discussed earlier, in the case of the tropical region this is typical of cumulus heating transport. Although it is well accepted that numerical simulations are very sensitive to the diabatic heating profile, e.g. Anthes

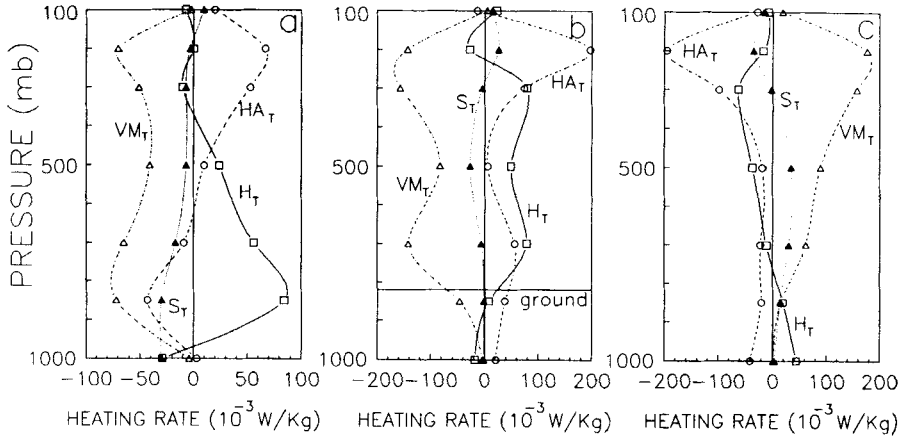

Figure 14. Vertical profiles of diabatic heating, H_T, (—□—□—□—); horizontal advection, HA_T, (○---○---○); vertical motion, VM_T, (△ - - △ - · - △); and storage term, S_T, (▲ · · · · ▲ · · · · ▲) for the composite Cyprus low at three selected gridpoints as follows: (a) 32.5°N, 35°E at the centre of the convective region in the cold front (point A in Fig. 8(e)); (b) 37.5°N, 42.5°E at the centre of the upward motion in the warm front (point B); (c) 35°N, 22.5°E at the centre of the downward motion in the wake of the cyclone (point C). Notice the different heating scales.

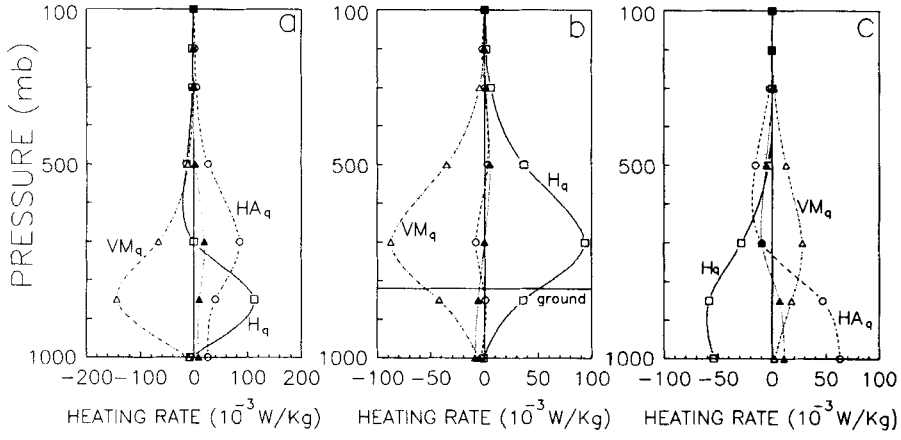

Figure 15. As in Fig. 14(a–c), but for the moisture budget terms.

and Keyser (1979), Bratseth (1985), Kanamitsu (1985), many studies have assumed a parabolic profile having a maximum in the upper half of the cloud (Reed and Recker 1971; Yanai *et al.* 1973; Kuo and Anthes 1984b). The present results show the importance of including a low-level heating profile in the models. Another point to be mentioned in Fig. 14(a) is that in the lower atmosphere the major term balancing the diabatic heating is the adiabatic cooling, VM_T, while in the upper troposphere the major heating term is the warm advection, HA_T. A significant differential temperature advection between 850 and 200 hPa levels indicates the developing stage of the cyclone according to quasi-geostrophic theory.

In the profile of the moisture terms a major vertical transport from the sea to the atmosphere, VM_q, reaching a maximum at 850 hPa, is balanced by a net sink, H_q, due to convection, while higher, at 700 hPa, the horizontal advection, HA_q, removes the moisture. This indicates that the sea is a moisture source not only for local convective clouds but also for the large-scale cloudiness.

Unlike the corresponding winter-averaged profiles in Figs. 5(a) and 6(a), the balances here for a composite Cyprus low reflect a very dynamical atmosphere with prominent convection. The adiabatic cooling, VM_T, attains a 800 hPa maximum value of -80×10^{-3} W kg^{-1} (Fig. 14(a)) as compared to only -10×10^{-3} W kg^{-1} for the average winter profile. The fact that the turbulent sea fluxes here are insignificant compared to those of the average winter is probably associated with point A being above the coast (35°E) and not right over the maximum sea fluxes at position 30°N, 27.5°E where the average winter profile has been presented.

Figure 14(b) shows the vertical variations of the heating terms at point B, right at the centre of the upward-motion region of the warm front (Fig. 8(e)). As discussed in section 4(b) the two maxima of the diabatic heating profile are typical for large-scale precipitation at the warm sector. The corresponding moisture profiles (Fig. 15(b)) clearly represent moisture transport upwards (VM_q) balanced by net condensation (H_q) very typical of tropical rain (see section 4(b)).

The profile of the heating terms at point C right at the maximum of downward motion is shown in Fig. 14(c). The diabatic heating term is dominated by radiative cooling with a maximum at the 300 hPa level where cloud tops like cirrus or cirrostratus are common. Only in the lower troposphere do the sensible heat fluxes make H_T positive. The profiles of the moisture terms (Fig. 15(c)) show a major moisture source (negative H_q) from the surface up to 500 hPa reflecting the turbulent-sea moisture flux. The vertical motion term, VM_q, removes moisture with a 700 hPa maximum, but the horizontal advection does the same only below about 800 hPa. The process of 'absorbing' moisture from the sea and carrying it by advection to the cyclone region is of major significance in cyclone evolution.

(*d*) *Comparison with the Baltic Sea*

A similar composite low for the Baltic Sea region was calculated and the average low centre was found at position 55°N, 17.5°E. The profiles of the horizontal advection and vertical motion terms are similar to those found for the Mediterranean, with one major exception: the diabatic heating is much smaller compared to the other terms (Fig. 16(a, b, c)) whereas in the case of the Cyprus low H_T is a most dominant term.

(*e*) *A single case-study, 6 January* 1987

The residual method in the present study could also be applied to a single case-study but the results are subject to major inaccuracies. Figure 17 shows a 1000 hPa typical

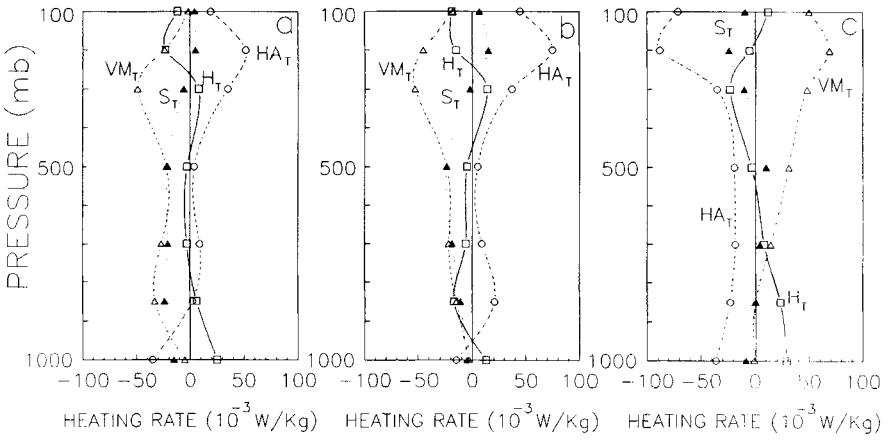

Figure 16. As in Fig. 14(a–c), but for the composite Baltic low centred over (55°N, 17.5°E) at the following gridpoints: (a) 55°N, 17.5°E; (b) 55°N, 25E; (c) 55°N, 2.5°E.

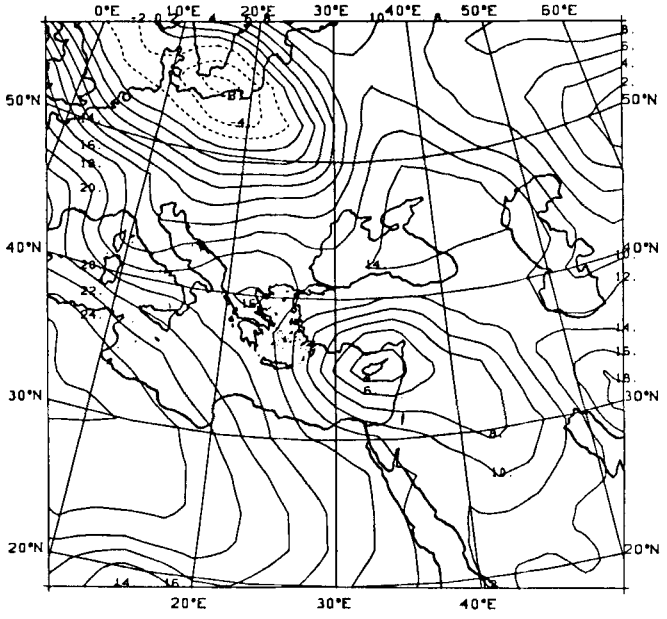

Figure 17. The 1000 hPa geopotential height for a typical Cyprus low on 6 Jan. 1987, 0000 UTC, based on ECMWF analysis. Positive (solid) and negative (dashed) contours are at intervals of 1 dam.

Cyprus low for 6 January 1987, 0000 UTC. The distribution of the integrated diabatic heating term, $[H_T]_p$, for this date is presented in Fig. 18 and is somewhat similar to that for the average Cyprus low (Fig. 9(a)), but with major differences. In the warm sector to the east (30°N, 42.5°E) the diabatic cooling may be too strong owing to the imbalance between the strong warm advection and the temperature change in 12 hours (see also Appendix 2). In the south-west sector (30°N, 27.5°E) the diabatic cooling seems too strong, probably because of exaggerated subsidence. The diabatic heating in the south-

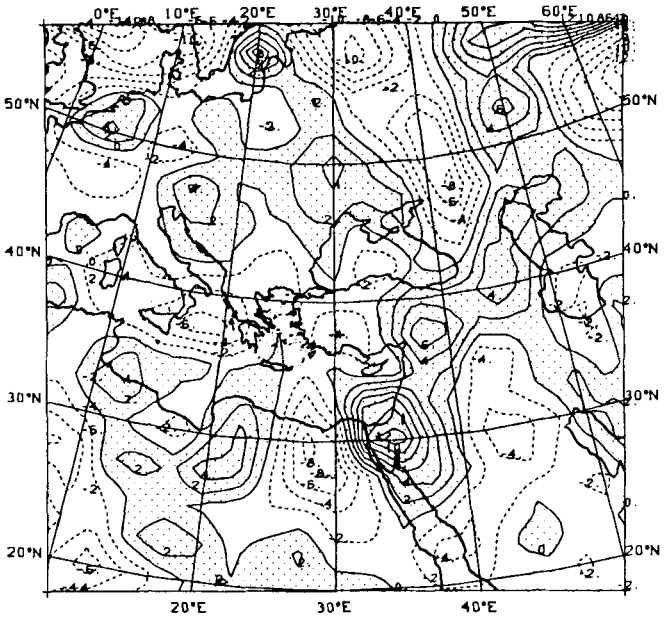

Figure 18. The vertically integrated diabatic heating, $[H_T]_p$, for the Cyprus low on the 6 Jan. 1987, 0000 UTC. Positive (solid) and negative (dashed) contours are at intervals of 2×10^2 W m^{-2}. Positive-value regions are shaded.

east, however, seems quite realistic when compared to the rainfall amounts reported on this date. The maximum of 1360 W m^{-2} corresponding to 25 mm/12 h is in good agreement with observations (maximum of 32 mm in Jerusalem). But the diabatic heating extends too much to the south and not enough to the west when compared with the rainfall distribution. Summarizing: the analysis of a composite Cyprus low helps to reduce errors and emphasizes the dominant features concerning the Cyprus low.

6. Conclusions

Based on the thermodynamic energy and the moisture balance equations, the residual method was employed in order to calculate the diabatic heating and net condensation terms over the Mediterranean region during winter. The horizontal and vertical distributions over the Mediterranean were compared with those over the tropics and over the North Sea for the purpose of identifying the physical role of diabatic processes in the Mediterranean with special emphasis on cyclonic activity in the eastern Mediterranean.

In comparing winter-averaged features, the Mediterranean was found to be characterized by prominent steady-state contributions as in the tropical region, but in contrast to the tropics the contributions by the transients in the Mediterranean, attributed to cyclone activity, are not at all negligible. As is the case for the North Sea, the transients in the Mediterranean do remove considerable heat and moisture from the water. The vertical profiles of the diabatic heating and net condensation show mainly the sea influence, i.e. heat and moisture subscale fluxes; but there is no prominent influence of the latent heat release.

A composite Cyprus low based on a large number of data-sets, with a significant cyclone centre over the eastern Mediterranean, was derived. The dynamic and thermodynamic structures of the Cyprus low were found and discussed. In particular, the close

association of a strong jetstream with the Cyprus low was found to be an outstanding feature.

The structure of the cyclone is reminiscent of that of a mid-latitude baroclinic quasi-geostrophic low but the importance of diabatic sources in the cyclone dynamics is much higher than in the northern latitude cyclone as noted in the following findings. Firstly, diabatic heating and net condensation distributions indicate vigorous sea fluxes, especially in the lee of the Turkish mountains over the Aegean sea where the contrast between the cold, dry air and the warm sea is maximized. Secondly, the latent heating reaches a maximum over the warm eastern sector of the cyclone along the southern slope of the mountain chain from Turkey to Kurdistan. This enhances the upward motion there, and probably plays a major role in cyclone development. Also, along the cold front over the south-eastern coast of the Mediterranean a second region of major latent heating was found and is probably associated with cumulus convection. Unlike other regions the maximum diabatic heating occurs at the lower altitude of about 850 hPa.

These results suggest topics for further study: for example, mesoscale modelling in which heating profiles corresponding to the present findings will be employed in order to understand better the complex role of the various physical processes in the Mediterranean.

Acknowledgements

The present work was supported by the BSF (Bi-national Israel–US Science Foundation) Grant No. 8600230. We thank the ECMWF for supplying the data, Dr B. U. Neeman for help with the graphics, Prof. B. Hoskins for encouragement during the initial stages, Rachel Duani for typing the manuscript and Z. Rosen for help in drafting Fig. 7. Prof. M. Podolak is thanked for reviewing the English grammar.

Appendix 1

Notation

C_q	Surface exchange coefficient for moisture
C_T	Surface exchange coefficient for heat
c	Condensation rate ($W\,kg^{-1}$)
c_p	Specific heat at constant pressure for dry air
e	Evaporation rate ($W\,kg^{-1}$)
F_q	Surface moisture flux ($W\,m^{-2}$)
F_T	Surface heat flux ($W\,m^{-2}$)
g	Acceleration of gravity ($m\,s^{-2}$)
H_q	Net sink term in the humidity equation ($W\,kg^{-1}$)
H_T	Diabatic heating term in the thermodynamic equation ($W\,kg^{-1}$)
HA_q	Horizontal advection term in the humidity equation ($W\,kg^{-1}$)
HA_T	Horizontal advection term in the thermodynamic equation ($W\,kg^{-1}$)
L	Latent heat of condensation of vapour to liquid ($2.5\times10^6\,J\,kg^{-1}$)
p	Pressure (hPa)
p_0	Reference pressure (1000 hPa)
p_s	Surface pressure (hPa)
p_t	Top pressure (100 hPa)
Q_R	Net radiative heating of air ($W\,kg^{-1}$)
q	Mixing ratio of water ($kg\,kg^{-1}$)
q_a	Mixing ratio at lowest free air level ($kg\,kg^{-1}$)

q_w Saturation mixing ratio of water surface (kg kg^{-1})
R_d Ideal gas constant for dry air (287 J kg^{-1} K^{-1})
S_q Storage term in the humidity equation (W kg^{-1})
S_T Storage term in the thermodynamic equation (W kg^{-1})
T Temperature
T_a Temperature of lowest free air level
T_w Temperature of water surface
t Time (s)
$\mathbf{V}$ Horizontal wind vector (m s^{-1})
VM_q Vertical motion term in the humidity equation (W kg^{-1})
VM_T Vertical motion term in the thermodynamic equation (W kg^{-1})
κ R_d/c_p (0.286)
ρ Air density (kg m^{-3})
θ Potential temperature (K)
ω Vertical velocity in pressure coordinates (Pa s^{-1})
$\langle\,\rangle$ Horizontal average
$(\,)_1$ Deviation from horizontal average
$\overline{(\,)}$ Time average
$(\,)^0$ Steady-state term
$(\,)^1$ Transient term
$[\,]_p$ Mass-weighted vertically integrated term

Appendix 2

Error estimation

There are three major error sources in calculating the diabatic heating and net condensation by the residual method from Eqs. (1) and (2): firstly, the inaccuracies in the basic ECMWF data-sets, secondly, the truncation errors due to finite difference approximations and thirdly, the errors arising from neglecting subgrid processes.

The inaccuracy of the ECMWF data depends mainly on density of observations. Assuming that the average error in the basic variables $\mathbf{V}$, ∇T etc. is of the order of 10%, the relative error in any of the terms in the equations becomes of the order of approximately 15%. Ignoring the storage term, which is in general very small, and assuming that the horizontal term is of the same order of magnitude as the vertical term, the residual error becomes of the order of 20% ($\sim(2^{\frac{1}{2}}\times 15)\%$) of any of the terms. That means, as long as the residual is larger than 40% of the largest term in the balance equation, the residual error due to data inaccuracies will not exceed 50%. Of course, this error could become even larger if errors in the basic variables are larger than 10% (as in the tropical regions, see section 3) or in data-sparse regions, but when the residual term is not too small compared to the other terms its relative error cannot be larger than that for these terms.

The truncation errors for $\partial F/\partial X$ by forward, centred and fourth-order centred finite differences is given by:

$$\frac{\Delta X}{2}\frac{\partial^2 F}{\partial X^2}, \qquad \frac{\Delta X^2}{6}\frac{\partial^3 F}{\partial X^3}, \qquad \frac{\Delta X^4}{30}\frac{\partial^5 F}{\partial X^5}$$

respectively. Assuming that

$$(\Delta X)^{n-1}\frac{\partial^n F}{\partial X^n} \sim \frac{\Delta F}{\Delta X}$$

for integral n, the accuracies are 50, 15 and 3 per cent respectively. Hence, the truncation error for the horizontal advection is $(2\frac{1}{2}\times 3)\% \cong 5\%$, 15% for the vertical motion and 50% for the storage terms (S_T, S_q).

The effect of subgrid processes was discussed throughout the work. The error arising from ignoring the subgridscale in connection with the time differencing term (storage) could become very large for a specific data-set, that means with no time-averaging. For example, at the front, advection is very strong but when the front moves relatively fast—compared to a time difference of 12 h—the corresponding heating does not reflect the high level of heating. Therefore, an artificial adiabatic cooling, balancing the advection, will be obtained: see e.g. the Cyprus low of 6 January 1987 described in section 5(e).

In summary, the calculated residuals are reliable if they are of the order of the advection and vertical motion terms but larger than the storage terms. In such circumstances the relative error is less than 50%.

References

Alpert, P. 1984 An early winter subtropical cyclone in the eastern Mediterranean, *Israel J. of Earth Sci.*, **33**, 150–156

Alpert, P. and Reisin, T. 1986 An early winter polar airmass penetration to the eastern Mediterranean. *Mon. Weather Rev.*, **114**, 1411–1418

Alpert, P. and Shay-El, Y. 1991 The paradox of the net moisture sink over the Arabian–Iraqi desert during winter *J. Clim.*, (in press)

Alpert, P. and Warner, T. T. 1986 Cyclogenesis in the eastern Mediterranean. Pp. 95–99 in WMO/TMP report series No. 22

Alpert, P., Neeman, B. U. and Shay-El, Y. 1990a Climatological analysis of Mediterranean cyclones using ECMWF data. *Tellus*, **42A**, 65–77

1990b Intermonthly variability of cyclone tracks in the Mediterranean. *J. Clim.*, **3**, 1474–1478

Anthes, R. A. and Keyser, D. 1979 Tests of a fine-mesh model over Europe and the United States. *Mon. Weather Rev.*, **107**, 963–984

Bengtsson, L., Kanamitsu, M., Kallberg, P. and Uppala, S. 1982 FGGE 4-dimensional data assimilation at ECMWF. *Bull. Am. Meteorol. Soc.*, **63**, 29–43

Bengtsson, L. 1988 Advances in the numerical prediction of the atmospheric circulation in the extratropics. Pp. 289–291 in Preprints, *Palmén Memorial Symposium on Extratropical Cyclones, Helsinki*, American Meteorological Society

Billing, H., Haupt, I. and Tonn, W. 1983 Evolution of a hurricane-like cyclone in the Mediterranean sea. *Beitr. Phys. Atmos.*, **56**, 508–510

Bratseth, A. M. 1985 A note on CISK in polar air masses. *Tellus*, **37A**, 403–406

Bultot, F. and Griffiths, J. F. 1972 The equatorial wet zone. Chapter 8 of *Climates of Africa*. Ed. J. F. Griffiths. Elsevier Publishing Company, Amsterdam, Netherlands

Charney, J. F. 1975 Dynamics of deserts and droughts in the Sahel. *Q. J. R. Meteorol. Soc.*, **101**, 193–202

Chen, T. C. and Baker, W. E. 1986 Global diabatic heating during FGGE SOP-1 and SOP-2 *Mon. Weather Rev.*, **114**, 2578–2589

El-Fandy, M. G. 1946 Baroclinic low of Cyprus. *Q. J. R. Meteorol. Soc.*, **72**, 291–306

Ernst, J. A. and Matson, M. 1983 A Mediterranean tropical storm? *Weather*, **38**, 332–337

Geller, M. A. and Avery, L. K. 1978 Northern hemisphere distributions of diabatic heating in the troposphere derived from general circulation data, *Mon. Weather Rev.*, **106**, 629–635

Hantel, M. and Baader, H. 1978 Diabatic heating climatology of the zonal atmosphere. *J. Atmos. Sci.*, **35**, 1180–1189

H.M.S.O. 1962 *Weather in the Mediterranean*, 2nd ed. Vol. 1. H.M.S.O.

Hollingsworth, A., Shaw, D. B., Lönnberg, P., Illam, L., Arpe, K. and Simmons, A. J. 1986 Monitoring of observations and analysis quality by a data assimilation system. *Mon. Weather Rev.*, **114**, 861–879

Holopainen, E. and Fortelius, C. 1986 Accuracy of estimates of atmospheric large-scale energy flux divergence. *Mon. Weather Rev.*, **114**, 1910–1921

Holton, J. R. 1979 *An Introduction to Dynamic Meteorology*, 2nd Ed. Academic Press, New York

Hoskins, B. J. and Berrisford, P. 1988 A potential vorticity perspective of the storm. *Weather*, **43,** 122–129

Hoskins, B. J. and Sardeshmukh, P. D. 1987 A diagnostic study of the dynamics of the northern hemisphere winter of 1985–1986. *Q. J. R. Meteorol. Soc.*, **113,** 759–778

Hoskins, B. J., Hsu, H. H., James, I. N., Masutani, M., Sardeshmukh, P. D. and White, G. H. 1989 Diagnostics of the Global Atmospheric Circulation based on ECMWF Analyses 1979–1989, WMO/TD No. 326, WCRP-27

Kallos, G. and Metaxas, A. 1980 Synoptic processes for the formation of Cyprus lows. *Revista di Meteorologia Aeronautica* **XL2–3,** 121–138

Kanamitsu, M. 1985 A study of the predictability of the ECMWF operational forecast model in the tropics. *J. Meteorol. Soc. Japan*, **63,** 779–804

Kasahara, A., Mizzi, A. P. and Mohanty, U. C. 1987 Comparison of global diabatic heating rates from FGGE Level III analyses with satellite radiation imagery data. *Mon. Weather Rev.*, **115,** 2904–2935

Krishnamurti, T. N., Low-Nam, S., Kumar, A., Sheng, J. and Sugi, M. 1987 Numerical weather prediction of monsoons. In *Monsoon Meteorology*. Eds. C.-P. Chang and T. N. Krishnamurti. Oxford Univ. Press, New York

Kuo, Y.-H. and Anthes, R. A. 1984a Accuracy of diagnostic heat and moisture budgets using SESAME-79 field data as revealed by observing system simulation experiments. *Mon. Weather Rev.*, **112,** 1465–1481

1984b Mesoscale budgets of heat and moisture in a convective system over the central United States. *Mon. Weather Rev.*, **112,** 1482–1497

Mayengon, R. 1984 Warm core cyclones in the Mediterranean. *Mar. Weather Log.* **28,** 6–9

Mizzi, A. P. and Kasahara, A. 1989 Intercomparison of daily values of atmospheric variables, including diabatic heating rates from the ECMWF, GFDL and GLA FGGE Level IIIb analyses. *J. Geoph. Res.*, **94,** 14717–14748

Petterssen, S. 1956 *Weather Analysis and Forecasting, Vol.* 1, *Motion and Motion Systems*. McGraw-Hill

Rasmussen, E. and Zick, C. 1987 A subsynoptic vortex over the Mediterranean Sea with some resemblance to polar lows. *Tellus*, **39,** 408–425

Reed, R. J. and Recker, E. E. 1971 Structure and properties of synoptic-scale wave disturbances in the equatorial western Pacific. *J. Atmos. Sci.*, **28,** 1117–1133

Tiedtke, M., Heckley, W. A. and Slingo, J. 1988 Tropical forecasting at ECMWF: The influence of physical parametrization on the mean structure of forecasts and analyses. *Q. J. R. Meteorol. Soc.*, **114,** 639–664

Trenberth, K. E. and Olson, J. G. 1988 An evaluation and intercomparison of global analyses from the National Meteorological Center and the European Centre for Medium Range Weather Forecasts. *Bull. Am. Meteorol. Soc.*, **69,** 1047–1057

Wallen, C. C. 1970 *Climate of Northern and Western Europe*, Elsevier Publishing Company, Amsterdam, Netherlands

Weare, B. C. 1988 Diabatic heating in the UCLA general circulation model. *J. Clim.*, **1,** 704–714

Yanai, M., Esbenson, S. and Chu, J. 1973 Determination of bulk properties of tropical cloud clusters from large-scale heat and moisture budgets. *J. Atmos. Sci.*, **30,** 611–627